A TRIDENT SCHOLAR PROJECT REPORT

NO. 467

Exploring the Propagation of the Madden-Julian Oscillation (MJO) across the Maritime Continent

by

Midshipman 1/C Casey R. Densmore, USN

UNITED STATES NAVAL ACADEMY
ANNAPOLIS, MARYLAND

USNA-1531-2

REPORT DOCUMENTATION PAGE

Form Approved
OMB No. 0704-0188

1. REPORT DATE *(DD-MM-YYYY)*
05-21-18

2. REPORT TYPE

3. DATES COVERED *(From - To)*

4. TITLE AND SUBTITLE
Exploring the Propagation of the Madden-Julian Oscillation (MJO) across the Maritime Continent

5a. CONTRACT NUMBER

5b. GRANT NUMBER

5c. PROGRAM ELEMENT NUMBER

6. AUTHOR(S)
Densmore, Casey R.

5d. PROJECT NUMBER

5e. TASK NUMBER

5f. WORK UNIT NUMBER

7. PERFORMING ORGANIZATION NAME(S) AND ADDRESS(ES)

8. PERFORMING ORGANIZATION REPORT NUMBER

9. SPONSORING / MONITORING AGENCY NAME(S) AND ADDRESS(ES)
U.S. Naval Academy
Annapolis, MD 21402

10. SPONSOR/MONITOR'S ACRONYM(S)

11. SPONSOR/MONITOR'S REPORT NUMBER(S)
Trident Scholar Report no. 467 (2018)

12. DISTRIBUTION / AVAILABILITY STATEMENT

This document has been approved for public release; its distribution is UNLIMITED.

13. SUPPLEMENTARY NOTES

14. ABSTRACT
The Maritime Continent (MC) is a region particularly susceptible to enhanced eastward-moving convective (thunderstorm) activity during the Madden-Julian Oscillation (MJO) active phase. To aid MJO predictability over the MC, atmospheric conditions across two vertical levels of the atmosphere were explored in this study: (a) humidity and height in the troposphere, and (b) wind in the stratosphere. In both, the Wheeler-Hendon Real-Time Multivariate MJO (RMM) Index was used to categorize MJO events over the MC from 1980-2017 based on their strength entering and exiting the region. An empirical orthogonal function analysis was developed to identify phases of the stratospheric Quasi-Biennial Oscillation (QBO) by direction and altitude of zonal wind centers. In the troposphere, positive specific humidity anomalies within the MJO active envelope and a near-surface "moisture foot" region in the lower troposphere east of the active envelope favor MJO propagation. In the stratosphere, east-west winds during active events can indicate the likelihood of intense, eastward-moving MJO thunderstorm intensity over the MC. These MJO events over the MC are likely to remain strong when easterly (westerly) mid-stratospheric QBO wind anomalies develop during boreal winter (spring and summer). When easterly mid-stratospheric wind anomalies are present, stratospheric temperature anomalies in thermal wind balance with the zonal wind anomalies decrease the upper-tropospheric and lower-stratospheric stability, aiding deep convection and favoring a stronger MJO. Mechanisms which explain the seasonality of this relationship are suggested areas for future research, as well as mechanisms which account for the boreal spring and summer QBO-MJO relationship.

15. SUBJECT TERMS
Large-scale tropical atmosphere, Climate dynamics, Madden-Julian Oscillation (MJO), Maritime Continent (MC), Specific Humidity, Quasi-Biennial Oscillation (QBO), Intraseasonal Variability

16. SECURITY CLASSIFICATION OF:			17. LIMITATION OF ABSTRACT	18. NUMBER OF PAGES	19a. NAME OF RESPONSIBLE PERSON
a. REPORT	b. ABSTRACT	c. THIS PAGE		51	19b. TELEPHONE NUMBER *(include area code)*

U.S.N.A. --- Trident Scholar project report; no. 467 (2018)

EXPLORING THE PROPAGATION OF THE MADDEN-JULIAN OSCILLATION (MJO) ACROSS THE MARITIME CONTINENT

by

Midshipman 1/C Casey R. Densmore
United States Naval Academy
Annapolis, Maryland

____

Certification of Adviser(s) Approval

Associate Professor Bradford S. Barrett
Oceanography Department

____

____

CAPT Elizabeth R. Sanabia, USN
Oceanography Department

____

____

Acceptance for the Trident Scholar Committee

Professor Maria J. Schroeder
Associate Director of Midshipman Research

____

____

USNA-1531-2

Abstract:

The Maritime Continent (MC) is a region particularly susceptible to enhanced convective (thunderstorm) activity during the Madden-Julian Oscillation (MJO) active phase. As the ascending branch of the MJO envelope reaches the MC, the convective signal may either propagate eastward through the MC and reach the Pacific Ocean (an active-to-active event) or weaken over the MC, not reaching the Pacific Ocean (an active-to-inactive event). Accurately predicting MJO amplitude changes over the MC is currently challenging, partially due to a lack of full understanding of atmospheric conditions that favor active MJO propagation. Determining differences in the background atmospheric state among these active-to-active and active-to-inactive events could aid understanding of the MJO, thereby increasing weather predictability in the MC and nearby regions critical to U.S. national security interests. To accomplish that objective, atmospheric conditions across two vertical levels of the atmosphere were explored in this study: (a) humidity and height in the troposphere, and (b) wind in the stratosphere. In both, the Wheeler-Hendon Real-Time Multivariate MJO (RMM) Index was used to categorize MJO events over the MC from 1980-2017 into one of four event types based on their amplitude entering and exiting the region. Standard anomalies of specific humidity and geopotential height were then computed using data from the European Centre for Medium-Range Weather Forecasts (ECMWF) ERA-Interim Reanalysis and compared among the four event types. Next, an empirical orthogonal function analysis was developed to identify phases of the Quasi-Biennial Oscillation (QBO) by direction and altitude of zonal wind centers. Impacts of the QBO on the upper troposphere and lower stratosphere that could serve as mechanisms for a QBO-MJO relationship were investigated. Finally, changes in MJO strength over the MC were compared to phase of the QBO in order to

determine potential relationships between the QBO and the MJO, and seasonality of this relationship was studied.

The results are as follows. First, the variability in active and inactive MJO events is both geographic and seasonal, and there are tropospheric and stratospheric environmental conditions that can help identify when intense MJO thunderstorm activity (an active MJO event) is likely over the Maritime Continent. Second, these MJO events are more likely to switch between active and inactive over the MC than over the Indian Ocean (IO) or western Pacific Ocean (WP). Furthermore, seasonal changes in MJO activity is diminished over the MC compared to the IO or WP. Third, there are tropospheric environmental characteristics unique to the MC during active events that indicate the likelihood of intense, eastward-moving MJO thunderstorm activity. Specific humidity anomalies are found to differ between active-to-active and active-to-inactive events, both within the MJO active envelope and in a "moisture foot" region in the lower troposphere east of the active envelope. Higher humidity in the moisture foot and active envelope favor MJO propagation. Moreover, the moisture foot signature is not present for active MJO events that remain active over the IO or WP, indicating that it is a feature unique to the MC. Finally, there are stratospheric wind conditions during active events that indicate the likelihood of intense, eastward-moving MJO thunderstorm intensity over the MC. These MJO events over the MC are likely to remain strong when easterly (westerly) mid-stratospheric QBO wind anomalies develop during boreal winter (spring and summer). When easterly mid-stratospheric wind anomalies are present, stratospheric temperature anomalies in thermal wind balance with the zonal wind anomalies decrease the upper-tropospheric and lower-stratospheric stability, aiding deep convection and favoring a stronger MJO. Results indicate that the seasonality of this relationship is due to seasonal differences in lower-stratospheric stability, MJO strength, structure, and propagation characteristics, as well as interactions with other atmospheric oscillations such as the diurnal precipitation cycle and Indian and East Asian Summer Monsoons. Mechanisms which explain the seasonality of this relationship are suggested areas for future research, as well as mechanisms which account for the boreal spring and summer QBO-MJO relationship.

Keywords: Large-scale tropical atmosphere, Climate dynamics, Madden-Julian Oscillation (MJO), Maritime Continent (MC), Specific Humidity, Quasi-Biennial Oscillation (QBO), Intraseasonal Variability

Acknowledgements:

The author gratefully acknowledges the continued support of his Trident advisors, Dr. Bradford Barrett and CAPT Elizabeth Sanabia. In addition, this project and associated conference travel were made possible due to funding from the USNA Midshipman Research Office and ONR award N0001416WX0175.

Table of Contents:

1. Introduction

Naval operations in the Maritime Continent and South China Sea rely on accurate weather predictions across multiple time scales (hourly, daily, weekly, and beyond) to effectively accomplish mission objectives. These operations can be negatively impacted by severe weather including thunderstorms and high winds and seas. A primary cause of severe weather in the region is the Madden-Julian Oscillation (MJO), which is currently difficult to predict as it crosses the island nations and archipelagos of southeastern Asia. Determining differences in background atmospheric conditions associated with different behaviors of the MJO can increase predictability of weather in this region, with impacts to both U.S. strategic interests and the global economy. The objective of this research is to better understand the behavior of the MJO and thereby improve predictability of severe weather in this operational theater.

A. The Madden-Julian Oscillation

The Madden-Julian Oscillation (MJO; Madden and Julian 1971, 1972) is the leading intraseasonal (30-60–day) mode of atmospheric climate variability. In other words, the MJO is the environmental phenomenon most responsible for changes in the weather within 30-60–day time frames (and indeed, the MJO was partially responsible for much of the sharp temperature contrasts over the eastern U.S. during February and March of 2018). The MJO consists of a broad circulation cell approximately 10,000 km in horizontal extent (Madden and Julian 1994) that propagates eastward along the equator and circumnavigates the globe in the tropics (Neale and Slingo 2003; Zhang 2005) over a period of approximately 30 to 60 days. The MJO circulation is comprised of upward motion on the western edge and downward motion on the eastern edge, and those updrafts and downdrafts are connected by winds toward the east aloft and toward the west at the surface

(Fig. 1). The region of upward motion (which will be referred to as the "active envelope" hereafter) is characterized by above-normal thunderstorm activity (a result of the strong upward vertical motion), and this region of enhanced convective activity results in above-normal precipitation and wind speeds that can negatively and unpredictably impact naval operations in this critical region. The region of downward motion (hereafter referred to as the "suppressed envelope") is characterized by below-normal precipitation and cloud cover due to MJO-induced sinking motion, or subsidence (Sperber 2003).

As a mode of intraseasonal variability, the MJO fits geospatially and temporally between the synoptic scale (e.g., frontal weather systems on the order of 100 km wide lasting several days) and the seasonal scale (e.g., differences between winter and summer) (Fig. 2). An important discovery within the past several decades is that the large amount of heat released by the thunderstorms in the MJO active envelope can influence weather patterns around the world, not just those in the tropics, including the timing and strength of the southeast Asian monsoon (Sui and Lau 1992), tropical cyclone formation and strength (Hall et al. 2001; Barrett and Leslie 2009), Arctic sea ice concentration (Henderson et al. 2014), global precipitation patterns (Zhang 2013), and severe weather patterns in the continental United States (Barrett and Gensini 2013; Barrett and Densmore 2016). The MJO can modulate these weather patterns around the world through physical processes in the atmosphere, most notably via atmospheric Kelvin and Rossby waves that propagate away from the active and suppressed envelopes. Atmospheric Kelvin waves are variations in surface (at altitudes of up to about 1 km) and upper-level (at altitudes of about 10 km) winds which propagate along boundaries (including the equator) with horizontal wavelengths (sizes) of approximately 1,000 km (Matsuno 1966). Atmospheric Rossby waves, however, move both east-west and north-

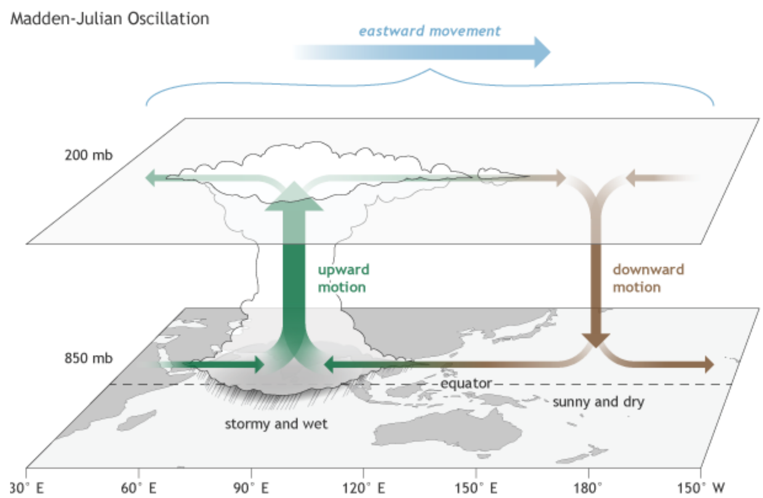

FIGURE 1: Atmospheric circulation and resultant convective activity typical of the active envelope of the MJO as it propagates through the MC. 2014 NOAA graphic by Fiona Martin.

south in the atmosphere, with wavelengths from 1,000 km to 10,000 km (Madden 1979). Both of these types of waves may propagate eastward and poleward away from the MJO active envelope, altering temperatures and upper-tropospheric winds around the globe (Zhang 2005).

The previously mentioned examples together highlight the importance for better understanding the MJO: it plays a key role in global weather and climate. Any Rossby or Kelvin waves excited by MJO convection will likely interact with other synoptic- to global-scale oceanic and atmospheric waves resulting from other oscillations, both in the tropics (about 23°S to 23°N) and away from tropical regions. The Quasi-Biennial Oscillation (QBO) is one such oscillation that exists independent of, yet interacts with, the MJO. The QBO is a thirty-month reversal in zonal winds in the equatorial stratosphere (Lindzen and Holton 1968; Baldwin et al. 2001; Fig. 3). Previous studies have observed a relationship between MJO timing and intensity and variability of QBO features. For example, Yoo and Son (2016) observed that MJO amplitudes are larger on average during the wintertime (December to February) QBO easterly phase (when winds in the stratosphere along the equator come from the east) than the westerly phase.

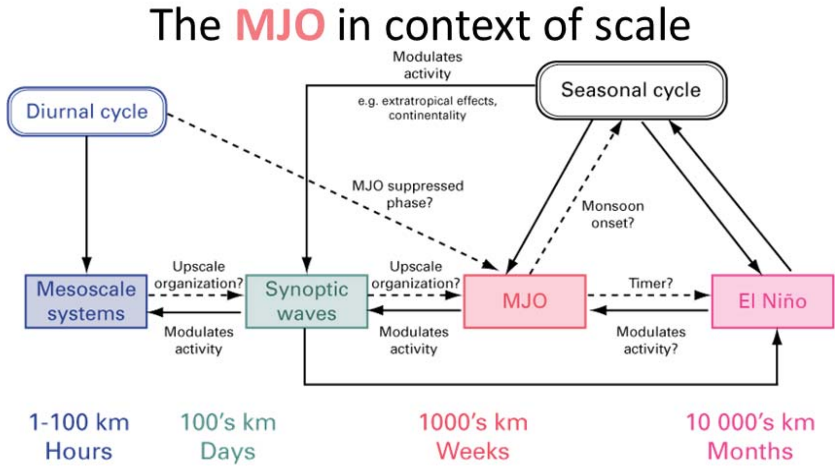

FIGURE 2: Positioning of the MJO in the major atmospheric temporal and spatial scales (adapted from Moncrieff et al. 2007).

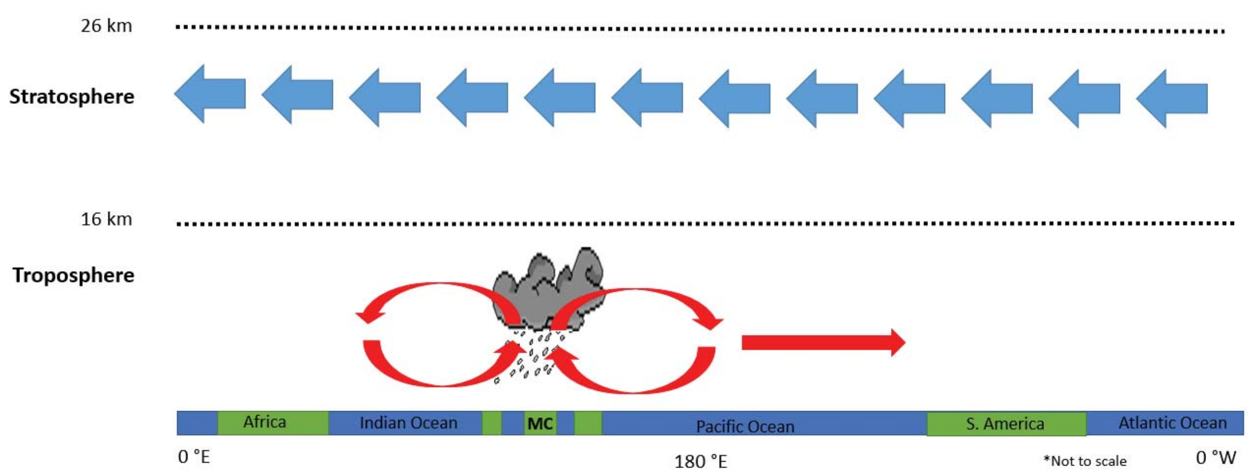

FIGURE 3: Zonal flow associated with the QBO (blue arrows represent flow associated with the easterly QBO) relative to MJO atmospheric circulation and convection (represented by the red arrows and cloud, respectively).

Studies analyzing the relationship between QBO and MJO have categorized the QBO by measuring the east-west winds at one pressure level (altitude) (e.g. 50 hPa, or about 19 km above the Earth's surface; Liu et al. 2014; Yoo and Son 2016; Marshall et al. 2016; Son et al. 2017; Nishimoto and Yoden 2017; Zhang and Zhang 2018). While this method identifies QBO-associated zonal wind direction in the middle of the stratosphere, it does not describe the full vertical structure of those winds. Because both easterly and westerly winds associated with the QBO descend through the stratosphere over time, limiting description of the QBO to a single level in the atmosphere may cause studies to miss important relationships between QBO and the MJO. Furthermore, because the stability (how prone an area is to thunderstorm activity) of the upper troposphere and lower stratosphere depends strongly on change in the zonal wind direction and speed with height (Baldwin et al. 2001), this detail may be important to the QBO-MJO association. To date, no known studies have found a QBO-MJO relationship beyond extended boreal winter (November through March). Finally, several recent studies examining the QBO-MJO relationship have reached conflicting conclusions, adding uncertainty to the meteorological community's understanding of the QBO-MJO relationship. Therefore, this Trident research addresses the need to continue to investigate that relationship, particularly using methods that identify the QBO at more than one altitude and across all seasons.

B. *Quantifying the MJO*

To help quantify the MJO and understand its interactions with the other atmospheric-oceanic oscillations discussed above, the MJO can be categorized into phases. One popular method to categorize MJO phase is empirical orthogonal function (EOF) analysis. The first two components of an EOF analysis can be used to identify the location and strength of the MJO. In the climate dynamics research community, one of the most frequently used MJO EOF analyses was developed by Wheeler and Hendon (2004; hereafter WH04), which they termed the Real-time Multivariate MJO (RMM) index. In WH04, whose index has been cited over 1590 times since 2004 by researchers studying the MJO, the authors defined MJO phase and amplitude using the two leading principal components of their EOF analysis, which was based on outgoing longwave radiation (OLR) and upper and lower atmospheric zonal (east-west) winds. Outgoing longwave radiation is measured by line-of-sight from a satellite to the earth. The OLR value recorded by the satellite is that of the first object between the satellite and the earth, i.e. the tops of clouds in cloudy areas and the earth's surface in cloud-free areas. Since there are strong relationships between the amount of radiation emitted by an object and its temperature, OLR can identify areas on earth with the highest clouds (where there is most likely strong thunderstorm activity). Therefore, an OLR minimum along the equator would indicate high clouds and deep thunderstorms, hence providing a locator to the strong updrafts on the western side of the MJO circulation. Likewise, a maximum in OLR would indicate an area without clouds and would typically be associated with the dry downdrafts on the eastern side of the MJO circulation.

The zonal (east-west) wind anomalies are important because they give insight into whether the upper-level eastward winds and lower-level westward winds are stronger than usual (indicating that the MJO circulation is present). When OLR and wind anomalies are weak, circulation around the MJO cell is also weak, and thus the MJO is deemed inactive (Liu et al. 2016). An active MJO was defined by WH04 as one with an RMM amplitude a greater than 1.0,

$$a = \sqrt{RMM1^2 + RMM2^2} \tag{1}$$

where *RMM1* and *RMM2* are the two leading principal components of the WH04 EOF analysis. An inactive MJO is one with RMM amplitude a less than or equal to 1.0. Thus, the daily WH04 RMM index approximates both the relative geographic position and intensity of the active and suppressed envelopes around the world (Fig. 4). On a phase-space diagram with *RMM1* and *RMM2* as x and y coordinates, a day with an active MJO will be located outside a unit circle with radius 1 (dark circle in center of Fig. 4 represents the threshold of active MJO). In April 2009 (red curve in Fig. 4), one of the most pronounced MJO events in the last 40 years moved eastward from the

Indian Ocean through the Maritime Continent (MC) and into the western Pacific Ocean. On 01 April 2009, the MJO was located in the Western Hemisphere and Africa (denoted by the word "START" and the small number 1, on the red curve in Figure 4). This MJO event moved east at a typical speed of around 5 m s^{-1}, crossing into the Indian Ocean (indicated as Phase 2 on Fig. 4) on 05 April 2009 (the date is indicated by the small number "5" along the red curve), then the MC (Phase 4) on 15 April 2009, finally reaching the Western Pacific (Phase 6) on 23 April 2009 (Fig. 4). The active envelope of this particular MJO event took 30 days to move from the Western Hemisphere (Phase 1) eastward around the globe to the Western Pacific (Phase 7). This type of MJO eastward propagation, and whether it continues to propagate eastward, weakens, or strengthens, is a core question of this Trident research effort.

Other indices have been developed since WH04 to quantify the MJO. One of these is the OLR MJO Index (OMI; Kiladis et al. 2014), which uses an EOF analysis of only bandpass-filtered OLR to project MJO strength and geographic position onto a phase space similar to the RMM index. The OMI index quantifies the MJO based on its convective anomalies (thunderstorm activity), but because of its focus on OLR, the OMI can fail to detect MJO-driven zonal wind features. Several recent studies (e.g. Yoo and Son 2016; Barrett et al. 2018; Zhang and Zhang 2018) have used both the RMM and OMI indices to describe MJO events and their relationships with other weather patterns. However, in boreal summer, both the RMM and OMI indices are less effective in identifying and classifying intraseasonal convection and wind activity (Lee et al. 2013). This uncertainty is related to the development of the Boreal Summer Intraseasonal Oscillation (BSISO; Lawrence and Webster 2002), the boreal summer counterpart to the MJO. The BSISO is a near- equatorial, northwestward-tilted band of convection that propagates

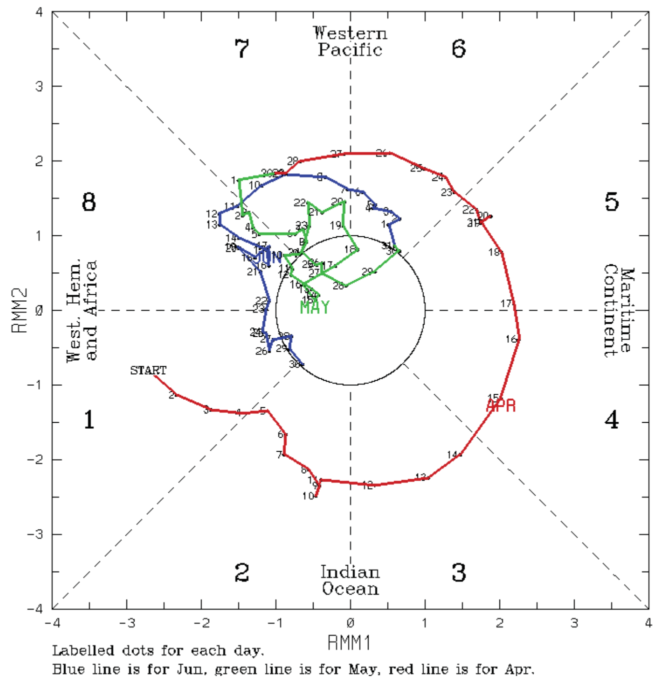

FIGURE 4: RMM Index for April 2009. Quadrant and distance from center for each point correspond to MJO location and strength for that day (Australian BOM website: www.bom.gov.au/climate/MJO).

northeastward across the MC and southeastern Asia away from the equator at a speed similar to the MJO. To capture this equatorially asymmetric, northeastward propagating convection, several additional indices have been developed (e.g. Lee et al. 2013; Kikuchi et al. 2012), and will be utilized in this research.

C. MJO propagation across the Maritime Continent (MC)

The MC is the equatorial region of island nations and archipelagos in Southeast Asia, including the Philippines, Indonesia, Malaysia, and Papua-New Guinea (Fig. 5), characterized by high atmospheric humidity and warm sea surface temperatures (Ramage 1968). Differential heating across the islands and adjacent warm seas drives an oscillating land-sea breeze, which creates convection (thunderstorms) and precipitation over land during the afternoon and over water at night (referred to as the diurnal cycle). As these thunderstorms develop, a large amount of latent heat is released via condensation (Ramage 1968). The diurnal cycle of thunderstorm activity in the MC is modulated by the MJO, as the thunderstorms associated with the MJO active envelope (updrafts on the west side of the MJO circulation) span such a broad region that they overwhelm the effects of the diurnal cycle, which happen on a smaller, mesoscale level (Fig. 2) (Inness and Slingo 2006). As a result, during the active MJO, thunderstorms are prevalent everywhere across the broad region of updrafts, instead of only developing over land during the afternoon and offshore during the overnight hours.

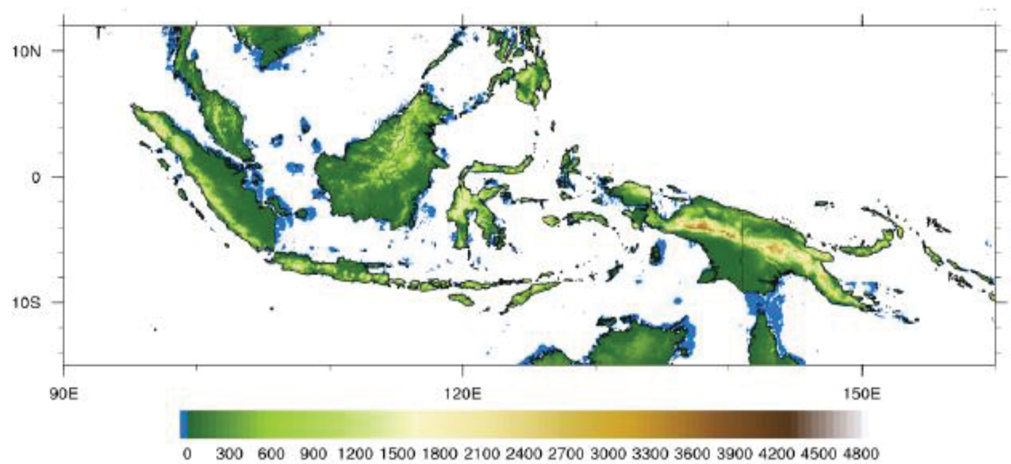

FIGURE 5: Maritime Continent boundaries and topography. Altitude is in meters (Ray et al. 2010)

As the MJO active envelope approaches the MC, it may propagate entirely across the MC while retaining its convective activity and continuing over the western Pacific Ocean (termed a propagating event). However, the convective activity may weaken (or even dissipate) over the MC (termed a non-propagating event) (Feng et al. 2015). These two types of MJO events are distinguishable in convection and atmospheric circulation (Fig. 6), as well as in meteorological variables such as humidity and geopotential heights. This study, which discriminates among MJO events based on their activity or inactivity upon entrance to and exit from the MC, terms propagating events as "active-active" (AA) events and non-propagating events as "active-inactive"

(AI) events. Conversely, when discriminating among MJO events which enter the MC inactive, those which develop activity are referred to as "inactive-active" (IA) events, and those which remain inactive are deemed "inactive-inactive" (IA) MJO events (Fig.6).

Atmospheric general circulation models (both weather and climate prediction models) currently show difficulty distinguishing between, and predicting, propagating and non-propagating events (Inness and Slingo 2006; Birch et al. 2016). Furthermore, the MJO research community does not yet fully understand the physical processes that differentiate propagating and non-propagating events (Kim et al. 2014). As such, MJO propagation across the MC is currently an active area of research. One potential distinguishing factor among MJO propagating and non-propagating events is the mean background atmospheric state during MJO passage. By determining differences in the background atmospheric state between propagating and non-propagating events, the physical processes which govern MJO propagation may be better understood. Furthermore, as these governing processes are better understood, the modelling community can use them to help diagnose reasons behind the MC predictability barrier (ONR 2015) and increase forecast accuracy

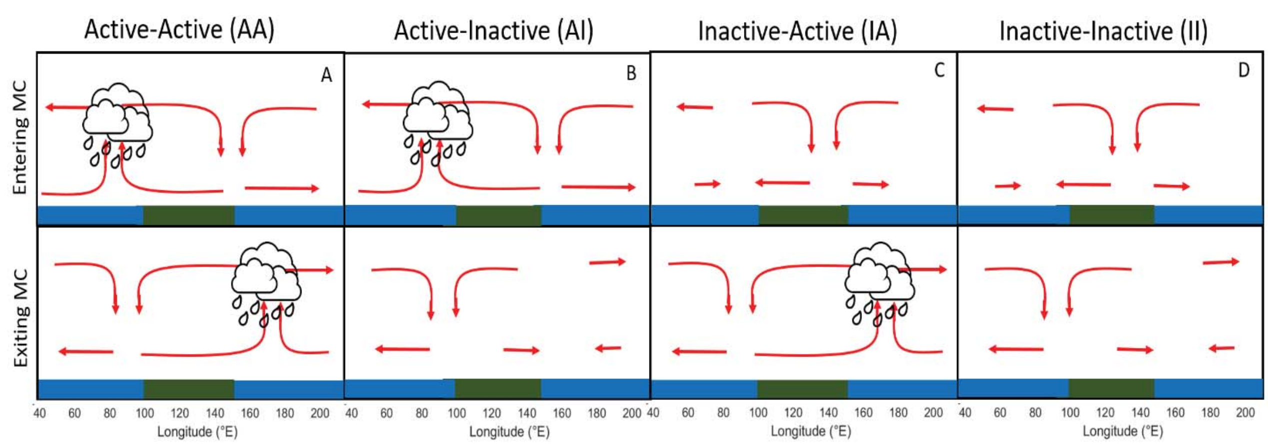

FIGURE 6: Zonal and vertical wind anomalies (red arrows) and resultant convective activity in each of the four cases of MJO events: active-active (AA, A), active-inactive (AI, B), inactive-active (IA, C), and inactive-inactive (II, D). Left and right blue shading represents the Indian and Western Pacific Oceans, respectively, and green shading represents the MC.

for global atmospheric models (Neena et al. 2014). This Trident research fills that need, investigating the differences in background atmospheric characteristics between propagating and non-propagating MJO events.

2. Objectives, Data, and Methods

The MJO propagation across the MC was the focal point of this study, specifically with regard to environmental characteristics (i.e., wind, humidity) that favor MJO activity and how they differ from those that favor inactivity, both in the troposphere and in the stratosphere. To do so, the study was divided into three research objectives:

A. Create a unique classification system for different MJO events and calculate frequency of each class, including seasonality

B. Identify differences in background atmospheric conditions over the MC in the troposphere and relate them to the MJO classes created in Objective A

C. Develop an index to classify the QBO, and use this index to analyze the relationship between phase of the QBO and the MJO.

The methodology for each of these objectives is detailed in the following subsections.

A. *Developing a classification system of MJO events categorized by shifts in activity*

The WH04 RMM index was used to classify MJO phases and amplitudes. The daily RMM index is available for download from the Australian Bureau of Meteorology's website (http://www.bom.gov.au/climate/mjo/). This index is a commonly used tool by forecasters around the world, a status achieved partly because it is available in real time and succinctly represents the most important aspects of the MJO. All MJO events from 1980-2015 were categorized based on their RMM amplitudes at the entrance to and exit from the MC in MJO phases 4 and 5, respectively, to reflect one of the four MJO cases detailed in Figure 5. Any MJO events too variable to define as one of the four MJO cases (either due to excessive reversal between activity and inactivity or insufficient eastward propagation; Roundy 2009) were excluded from categorization and subsequent analysis. An idealized representation of the RMM index signatures for these four MJO events is shown in Figure 7.

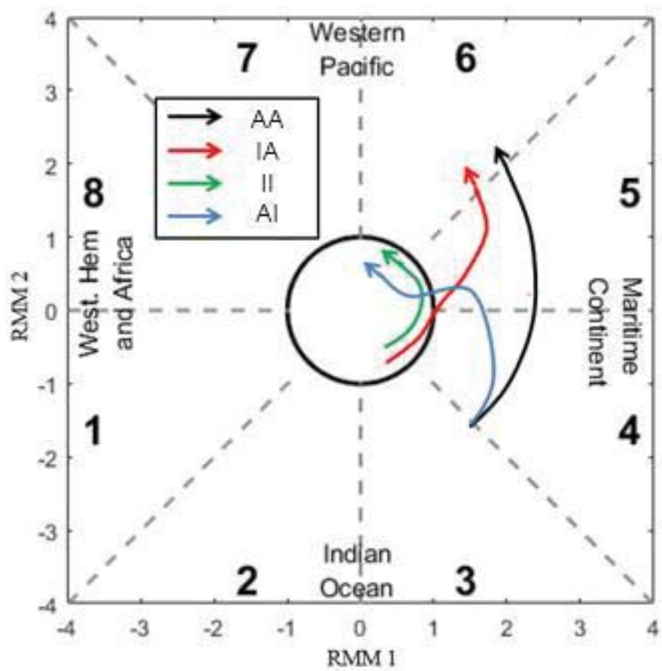

FIGURE 7: Idealized WH04 RMM signatures for each of the four cases of MJO events over the MC.

Active-active (AA) events entered and exited the MC (MJO phases 4 and 5, respectively, on the RMM index) with RMM amplitudes greater than 1 and were required to maintain those amplitudes for at least 80% of their time in the MC. Active-inactive (AI) events entered the MC with RMM amplitudes greater than 1, but exited with amplitudes less than 1. Inactive-active (IA) events entered the MC with RMM amplitudes less than 1 but developed RMM amplitudes greater than 1 while over the MC and exited the MC with RMM amplitudes greater than 1. Finally, inactive-inactive (II) events entered and exited the MC with RMM amplitudes less than 1, and were required to retain amplitudes less than 1 for 80% of their time in the MC. In order to be considered for analysis, MJO events also had to demonstrate eastward propagation (counterclockwise in RMM phase space; Fig. 7) on a day-to-day basis for at least 65% of days while over the MC. This threshold was selected because it eliminated events whose RMM index profiles lacked a strong MJO signature and included events that exhibited eastward propagation. This process was repeated for MJO events over the Indian Ocean (hereafter IO) for MJO phases 2 and 3 and the western Pacific Ocean (hereafter WP) for MJO phases 6 and 7.

This analysis was then replicated using the outgoing longwave radiation (OLR) MJO Index (OMI, Kiladis et al. 2014). MJO categorization was very similar between the two indices, even though the RMM weighs winds more and the OMI uses only OLR. The agreement between the two indices increased confidence in the results and enables them to be applied to forecasts of the MJO. MJO case categorization using the OMI index is similar to categorization using the RMM index, confirming the ability of the RMM index to capture the convective signature of the MJO.

B. Calculating standard anomalies of the background atmospheric state

To compare the mean background atmospheric state among MJO cases, specific humidity (q) and geopotential height (ϕ) from the European Centre for Medium Range Weather Forecasts (ECMWF) ERA-Interim reanalysis (Dee et al. 2011) were compared for the four MJO cases. Daily data at 0000 UTC and 1200 UTC from 01 January 1980 – 31 December 2015, bounded meridionally by 15°S to 15°N and zonally with an eastern boundary of 140°W and a western boundary of 0°E, were analyzed. The ERA-Interim reanalysis data are available for download from the ECMWF archive (www.ecmwf.int/en/forecasts/datasets/reanalysis-datasets/era-interim). The 0000 UTC and 1200 UTC hours were selected because the Indonesian Agency for Meteorology, Climate, and Geophysics (BMKG) regularly collects radiosonde observational data at numerous weather stations across the MC at 0000 UTC and 1200 UTC (observations which contribute to the reanalysis products to be used in this research). A five-day running mean was applied to the reanalyses to remove high-frequency (short-term) atmospheric variability. Standard anomaly composites were calculated for each of the four MJO cases as the difference between a variable at a date and time and the monthly mean, divided by the standard deviation of the monthly mean. For example, specific humidity standard anomalies were calculated as follows:

$$q_{stdanom_i} = \frac{q_{i,j} - \mu_j}{\sigma_j} \tag{2}$$

in which $q_{i,j}$ represents the specific humidity anomaly at day *i* and month *j*, μ_j is the climatological mean of specific humidity for month *j* for 1980-2015 (the period of MJO events analyzed), and σ_j is the standard deviation of the specific humidity for month *j* used to compute the climatological mean. Standard anomalies were calculated for specific humidity and geopotential height upon MJO entrance to the MC, IO, and WP (depending on the location of the MJO event analyzed), as well as the eight days prior to and the eight days after MJO entrance to the MC, IO, and WP. Standard anomaly composites were produced by averaging anomalies for each MJO case, creating 36 composites for each variable: one for each of the four MJO cases (AA, AI, IA, and II) in the three regions (MC, IO, and WP) for each of three days (day -8, day 0, and day +8) analyzed.

Outgoing longwave radiation (OLR) standard anomaly composites were calculated using Equation 2 and data from NOAA Earth Systems Research Laboratory (available at https://www.esrl.noaa.gov/psd/data/gridded/data.interp_OLR.html), for 1980-2013 (limited to

2013 by the span of the dataset). These composites were compared between AA and AI cases for each of the three regions (MC, IO, and WP). The composites highlighted the convective activity associated with the MJO, provided the broad location of maximum convection for each region, and showed differences in convection between initially active propagating (AA) and non-propagating (AI) events. Analyzing OLR signatures from MJO events classified using the RMM index also served as an additional method of validating use of the RMM index to accurately capture the MJO convective signature. Specific humidity, geopotential height, and OLR standard anomalies were tested for statistical significance at the 95% confidence level with a two-tailed student's *t* test.

Finally, to contrast active (inactive) events, AI (II) anomalies were subtracted from AA (IA) anomalies. This analysis was completed for all three variables (specific humidity, geopotential height, and OLR). The differences between population means were tested for statistical significance at the 95% confidence level using a Welch's *t*-test, where significance was indicated when $z \geq t$. In this case, t was the rejection t value, conservatively estimated as the inverse t value for the lower number of degrees of freedom among the two populations. The test statistic z was calculated as follows:

$$z = \frac{\overline{x_a} - \overline{x_b} - \Delta}{\sqrt{\frac{{\sigma_a}^2}{N_a} + \frac{{\sigma_b}^2}{N_b}}} \tag{3}$$

where $\overline{x_a}$ and $\overline{x_b}$ represent the means of populations a and b, Δ represents the theoretical difference of the means in the null hypothesis ($\Delta = 0$ for the population mean difference tests in this study), σ_a and σ_b are the standard deviations of populations a and b, and N_a and N_b are the sample sizes of populations a and b. Differences which met the criteria $z \geq t$ were considered to be points where the population means were significantly different from one another.

C. Comparing QBO phase to the MJO

The QBO is classified using an empirical orthogonal function (EOF) analysis of daily zonal wind anomalies from 1980-2017 (similar to Fraedrich et al. 1993 and Wallace et al. 1993), using stratospheric zonal wind observations from the ECMWF ERA-Interim Reanalysis (Dee et al. 2011; www.ecmwf.int/en/forecasts/datasets/reanalysis-datasets/era-interim). Unlike the RMM index, whose PCs were determined by an EOF in WH04, this index is developed for this analysis to detect potential relationships between the MJO and the QBO. The wind data were averaged across the equator from 10°S to 10°N, included all longitudes and was bounded vertically by 100 hPa and 10 hPa (corresponding roughly to 16 and 31 km altitude, respectively). This approach limited the analysis to the stratosphere. Zonal wind data are smoothed across time using a 151-day running mean filter in order to remove variability from weather patterns on seasonal and shorter timescales, following Wallace et al. (1993) Wind anomalies used in the analysis are calculated relative to a 31-day climatological (1980-2017) sliding mean, that is, the mean wind speed for the 15 days prior to and after a given day is subtracted from the winds at that day in order to remove the effect of season.

Variance of the first ten principal components produced by this EOF analysis is presented in Figure 8a. The first three principal components account for 15%, 12%, and 3% (respectively) of the total variability in stratospheric zonal wind anomalies, with higher-order principal components accounting for decreased variability (Fig. 8a). The variability captured by the first two principal components is centered on the 2-3–year time period (Figure 8b), which corresponds well to the mean periodicity of the QBO (Lindzen and Holton 1968; Baldwin et al. 2001). Specifically, 50% of the variability in the first principal component and 53% of the variability in the second principal component exist within this time window. This observation suggests that most of the changes in those first two components can be attributed to oscillations with periods that fall between two and three years, the QBO's timescale. Less than 15% of the variability in subsequent principal components falls within the QBO's timescale, and therefore, those principal components will not be analyzed further. Finally, daily time series of the first two principal components, divided by their standard deviation (normalized) and hereafter labelled QBO1 and QBO2, are presented in Figure 8c. These principal components oscillate with a period of approximately 2.5 years, and are offset by approximately 90°, indicating their orthogonality. Therefore, these first two principal components capture complementary variability of stratospheric winds, and together account for 27% of stratospheric zonal wind variability in the tropics.

The first two normalized principal components result in a QBO phase space (Figure 9) from which the QBO winds can be interpreted. The angle around the center of the diagram indicates the altitude and direction of the stratospheric zonal winds (annotated on the figure), and the distance from the center corresponds to wind speed. As the QBO winds move downward through the stratosphere, the winds' respective locations on the figure move counterclockwise around the phase space, completing one revolution every 2.5 years. Based on the angle in the phase space, the stratospheric wind profile generated by the QBO is divided into eight phases (separated on Figure 9 by dashed grey lines, labelled A-H). These QBO phases are grouped in pairs by direction and approximate altitude of zonal wind centers, a technique which also increases sample size and thus statistical significance of the results. QBO phases H and A represent days with lower-stratospheric westerly wind anomalies (annotated in blue, and hereafter annotated as QBOWL). QBO phases B and C represent days with mid-stratospheric easterly winds (annotated in green, hereafter QBOEM). QBO phases D and E represent days with lower-stratospheric easterly winds

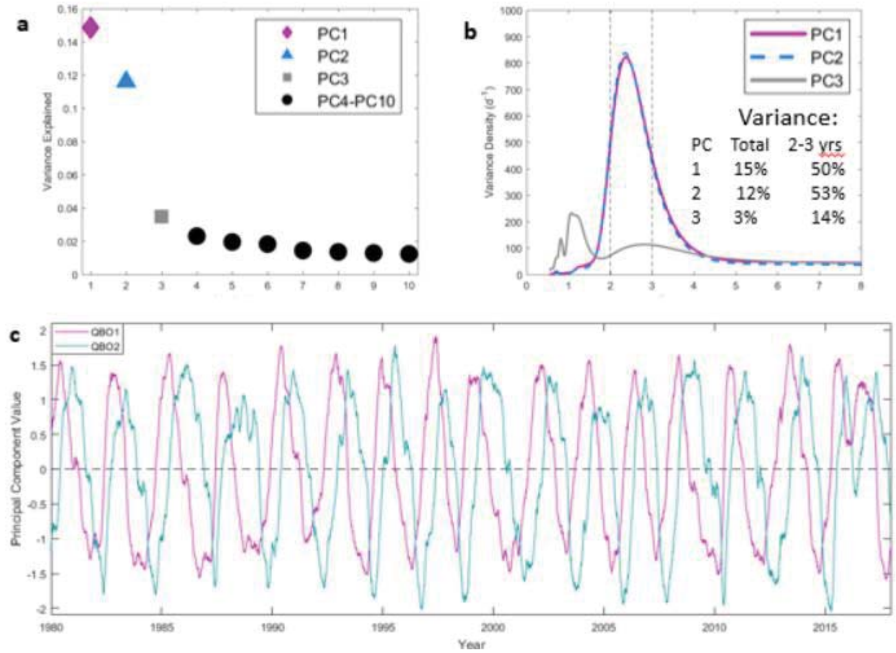

FIGURE 8: (a) Total variance of stratospheric winds from 1980-2017 accounted for by the first ten principal components of the EOF analysis, (b) variance density spectra of the first three principal components, and (c) daily time series of the first two principle components, normalized by their respective standard deviations (QBO1 and QBO2, respectively). Vertical lines in panel b denote periods between 2 and 3 years.

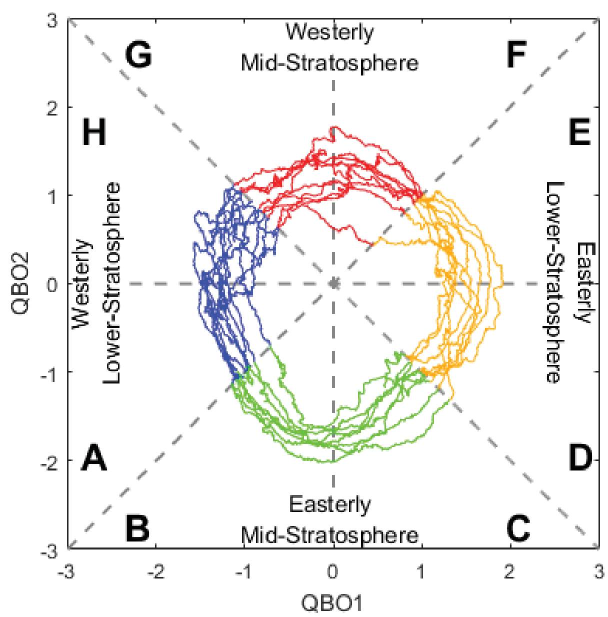

FIGURE 9: Phase space diagram of QBO1 and QBO2 from 1980-2017. Eight phases (separated by dashed lines) divide the QBO zonal winds by direction and altitude of the wind maxima. Distance from the center of the figure corresponds to zonal wind anomaly magnitude. Similar QBO wind profiles are binned into four phase-pair subsets, denoted by color as: blue (Westerly Lower-Stratosphere; QBOWL), green (Easterly Mid-Stratosphere; QBOEM), orange (Easterly Lower-Stratosphere; QBOEL), and red (Westerly Mid-Stratosphere; QBOWM).

(orange, hereafter QBOEL), and QBO phases F and G represent days with mid-stratospheric westerly winds (red, hereafter QBOWM).

During their movement through RMM phases 2 through 7 (corresponding to MJO passage from the Indian Ocean, through the Maritime Continent, and over the western Pacific Ocean), mean amplitude of MJO events are analyzed for each QBO phase pair in Section 3C. To reduce the effects of the number of active MJO days and the MJO propagation speed (which had a strong effect on the QBO-MJO relationship; Zhang and Zhang 2018), RMM amplitudes for each event are binned by and averaged for the entrance and midpoint for each MJO phase. Then, those mean entrance and midpoint amplitudes are then averaged together for all MJO events in each QBO phase. In addition, to isolate the effects of active MJOs, all days where the RMM amplitude was less than 1 are excluded (thereby focusing the study on not only MJO events but also on events that maintained an RMM amplitude of greater than 1). Statistical significance is tested using a Welch's *t* test (Son et al. 2017) to identify significant differences in MJO amplitude among QBO phase pairs at the 95% confidence level. Mean MJO amplitude changes for events over the MC, averaged by QBO phase pair, are presented for the 42 MJO events which occurred during boreal winter. This analysis is repeated for the 35 boreal winter MJO events identified propagating as active through the MC with the OMI index.

Finally, seasonality of MJO amplitude change over the MC by QBO phase pair for each seasonal subset is presented. During boreal summer (June through August), amplitude changes for both the WH04 RMM index and a BSISO index are presented. The BSISO index (Kikuchi et al. 2012) is designed to better capture seasonal shifts in MJO-related thunderstorm activity propagation and structure during boreal summer. This seasonality analysis was repeated using the OMI Index (Kiladis et al. 2014), to compare to results obtained with the RMM index.

To better understand the physical mechanisms for the observed QBO-MJO and QBO-BSISO relationships, zonal wind speeds, Brunt-Väisälä (BV) frequencies and anomalies, zonal wind shear values, and temperature anomalies for each QBO phase pair are examined. Vertical profiles of each of these variables and parameters are calculated using data from 1980-2017 from the ERA-Interim Reanalysis. These parameters are averaged for the entire world between 10°S to 10°N, and bounded vertically by 100 hPa and 10 hPa. The BV frequency is a measure of atmospheric stability, where unstable conditions are associated with thunderstorm activity and stable conditions are associated with calm weather. Lower BV frequencies correspond to less stable conditions which favor enhanced thunderstorm activity (and in this case, stronger MJO active envelopes), and vice versa. In this study, BV frequency was calculated as:

$$N^2 = \frac{g}{\theta}\left({}^{\delta\theta}/_{\delta z}\right) \tag{4}$$

where g is the gravitational constant 9.8 m^1 s^{-1}, θ is the potential temperature, and ${}^{\delta\theta}/_{\delta z}$ is the change in potential temperature with height (Stull 1995). To consider potential seasonality of the QBO-MJO relationship, MJO amplitude change and effects of QBO on zonal wind shear and BV frequency were analyzed by seasonal subsets: boreal winter (December, January, and February; DJF), boreal spring (March, April, and May; MAM), boreal summer (June, July, and August; JJA), and boreal autumn (September, October, and November; SON).

3. Results

A. *MJO case frequency and propagation*

From 1980-2015, 199 MJO events were identified over the MC using the RMM index (Fig. 10). Of those 199, 132 entered the MC classified as active. There were 92 events that remained active while propagating through the MC (AA events, Fig. 10A), and the other 40 events became inactive (AI events, Fig. 10B). Of the remaining 67 events which entered the MC while inactive, 30 events developed activity over the MC (IA events, Fig. 10C), and the other 37 events never developed activity (II events, Fig. 10D). Additionally, 159 MJO events were identified over the IO during the same time period (Fig. 11). Of these events, 98 entered the IO active, including 75 AA events (Fig. 11A) and 23 AI (Fig. 11B) events. Out of the remaining 61 MJO events, 21 were classified as IA (Fig. 11C) and 40 were classified as II (Fig. 11D). Finally, 191 total MJO events were identified over the WP from 1980-2015 (Fig. 12). There were 129 MJO events that entered the WP active, of which 103 were AA events (Fig. 12A) and 26 were AI events (Fig. 12B). The remaining 62 MJO events entered the WP inactive, of which 15 were IA events (Fig. 12C) and 47 were II events (Fig. 12D).

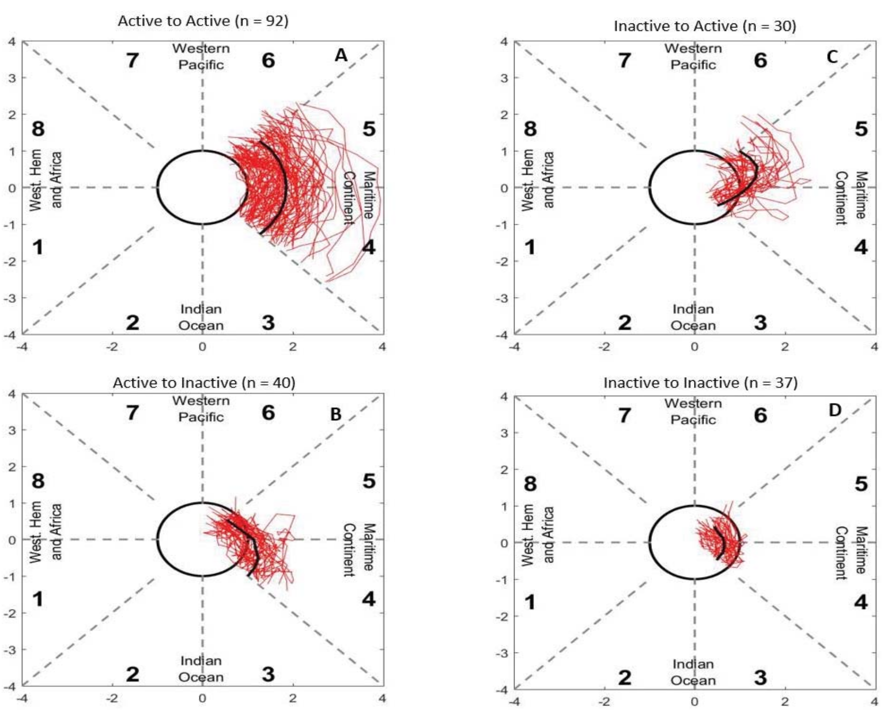

FIGURE 10: MJO events over the Maritime Continent (MJO phases 4 and 5) from 1980-2015, categorized as either active-active (AA,a), active-inactive (AI, b), inactive-active (IA, c), or inactive-inactive (II, d). Black lines denote case averages.

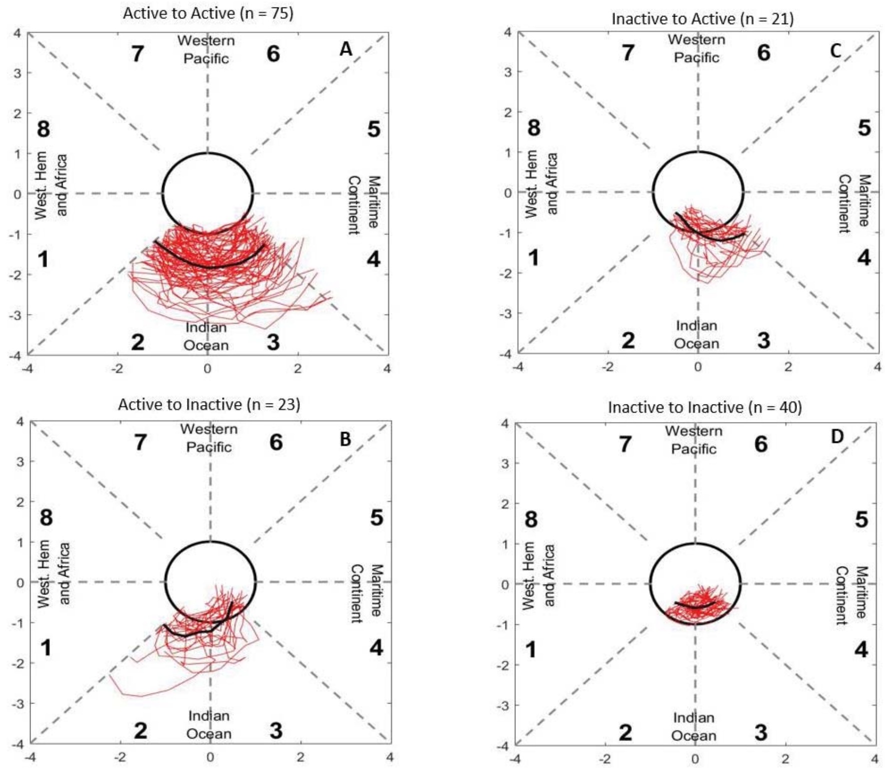

FIGURE 11: As in Figure 6, but for MJO events over the Indian Ocean (MJO phases 2 and 3).

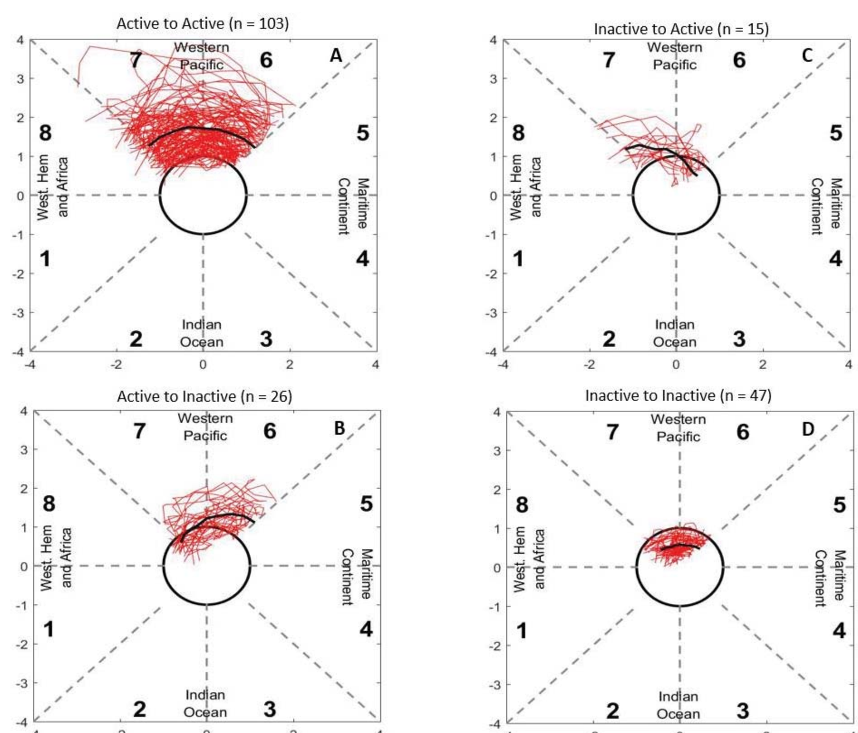

FIGURE 12: As in Figure 6, but for MJO events over the western Pacific Ocean (MJO phases 6 and 7).

The MJO case occurrences among the MC, IO, and WP are presented in Table 1. The likelihood of MJO propagation given its starting amplitude is greater over the MC than either the IO or WP. Over the MC, 132 events (66% of all MJO events over the MC) enter the region as active. Of these 132 events, 70% remain active while over the MC (AA) and the other 30% of events become inactive (AI). However, only 23% of initially active events over the IO and 20% of the same events over the WP become inactive (AI). Therefore, initially active events are more likely to become inactive over the MC than the IO or WP.

Of the remaining 67 events (34% of all MJO events) over the MC which enter as inactive, 45% become active while over the MC (IA) and the other 55% of events remain inactive (II). However, initially inactive MJO events over the IO and WP are less likely to become active over the IO and WP than the MC, with 34% of inactive events over the IO and 24% of the same events over the WP developing activity (IA). Therefore, inactive events are more likely to develop activity over the MC than the IO or WP. Overall, MJO events are more likely to switch from active to inactive, or inactive to active, while propagating over the MC than either the IO or WP.

MJO event frequency also varies with season (Table 2). Over the MC, during boreal winter (DJF), 66% of MJO events that enter active exit active (AA), whereas during boreal summer (JJA), only 52% of such events exit active (AA). This seasonal difference is even more pronounced over the IO and WP. Initially active events over the IO propagate successfully 80% of the time (AA) during boreal winter, but only 56% of the time during boreal summer. Initially active events over the WP propagate successfully 91% of the time (AA) during boreal winter, but only 68% during boreal summer. These differences suggest that in boreal winter (DJF), events entering active are less likely to exit active in the MC than in the IO or WP (66% compared to 80% and 91%, respectively). Seasonality of MJO propagation and intensification over the MC highlights the need for a better understanding of MJO propagation, particularly given that the seasonality also differs between the MC and the IO and WP. Propagation and non-propagation of MJO events are potentially related to the background atmospheric state, interannual variability, or a combination thereof.

TABLE 1: Comparison of mean initial amplitude ($\bar{x}$) for MJO events identified from 1980-2015 for the Maritime Continent (MC, phases 4 and 5, n = 199), Indian Ocean (IO, phases 2 and 3, n = 159), and western Pacific Ocean (WP, phases 6 and 7, n = 191). MJO event classifications are based on RMM amplitudes at entry to and exit from their respective regions.

Enter \ Exit		ACTIVE			INACTIVE		
		MC	IO	WP	MC	IO	WP
ACTIVE		AA			AI		
	$\bar{x}$ =	**1.80**	**1.65**	**1.71**	**1.44**	**1.47**	**1.57**
	n =	92	75	103	40	23	26
INACTIVE		IA			II		
	$\bar{x}$ =	**0.74**	**0.71**	**0.65**	**0.65**	**0.62**	**0.63**
	n =	30	21	15	37	40	47

TABLE 2: Occurrences of different MJO propagating cases (AA, AI, IA, II, all defined in Table 1 and text) by season for each region (MC, IO, WP).

	AA			**AI**			**IA**			**II**		
	MC	IO	WP	**MC**	IO	WP	**MC**	IO	WP	**MC**	IO	WP
Entire Year	**92**	75	103	**40**	23	26	**30**	21	15	**37**	40	47
DJF	**26**	20	31	**13**	5	3	**4**	5	4	**11**	7	11
MAM	**29**	30	34	**11**	6	6	**6**	5	5	**11**	7	14
JJA	**12**	9	13	**11**	7	6	**10**	5	2	**8**	16	14
SON	**25**	16	25	**5**	5	11	**10**	6	4	**7**	10	8

B. Differences in background atmospheric state among MJO cases

One way to discriminate between AA, AI, IA, and II cases is to look for differences in the atmospheric state before, during, and after propagation. Specific humidity and geopotential height anomalies thus are analyzed to better understand MJO propagation across the MC. The AA and AI MJO events exhibit significant differences as they approach the western boundary of the MC (Fig. 13). The active envelopes of AA MJO events are characterized by specific humidity differences up to 0.5 standard anomalies greater than AI events (Fig. 13F). In addition, negative low-level geopotential height anomalies are –0.3 standard anomalies lower, and positive upper-level geopotential height anomalies are and +0.1 standard anomalies greater, in AA events than in AI events (Figs. 13A,B). This difference suggests that the active envelope is more humid and stronger in AA cases than AI cases when entering the MC on day 0, even though both enter the MC with similar RMM amplitudes. Moreover, there is a significant low-level positive humidity anomaly extending over the MC, and this moisture foot signature is present for both AA and AI MJO events propagating over the region. However, humidity anomalies are 0.3 standard anomalies more positive for AA MJO events than AI events.

This moisture foot signature is not present in initially active MJO events propagating over the IO (Figs. 14C, D) or WP (figure not shown). In addition, moisture anomalies in the MJO active envelope vary much less between AA and AI cases over the IO than over the MC. However, statistically significant negative low-level geopotential height anomalies (-0.9 standard anomalies) exist by day 0 for AA events over the IO. These anomalies are significantly more negative (by 0.3 standard anomalies) than lower-level geostrophic height anomalies for AI events (Fig. 13F). Together, these results highlight the importance of specific humidity and geopotential heights as potential precursors for successful eastward MJO propagation over the MC: propagating events are more humid both in the active envelope and the moisture foot, and propagating events have lower geopotential heights in the lower troposphere over the MC.

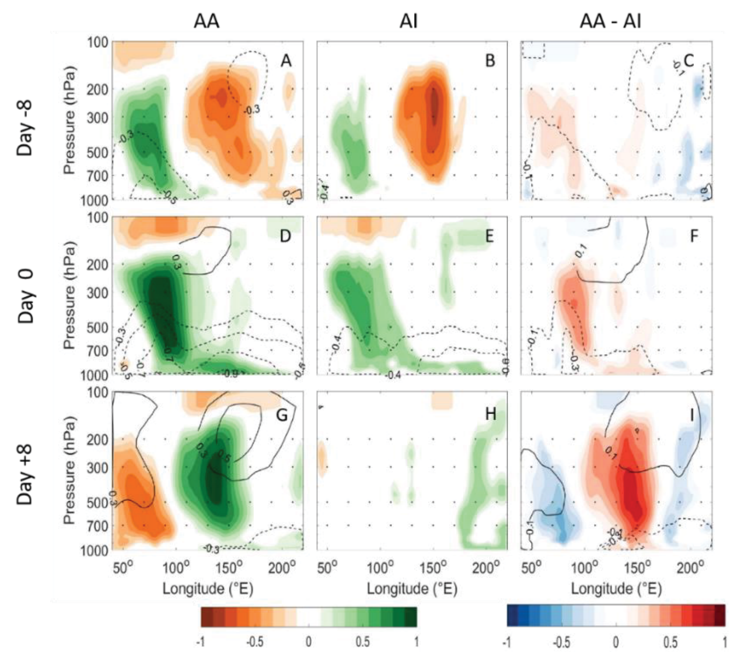

FIGURE 13: Specific humidity (color-filled) and geopotential height (unfilled contours, positive represented by solid lines) standard anomaly contours averaged from 15 °S to 15 °N as the MJO active envelope crosses the western boundary of the MC (100 °E). Anomalies are shown for AA (A, D, G) and AI (B, E, H) MJO events, as well as the differences between the two (C, F, I) at -8 (A-C), 0 (D-F), and 8 (G-I) days relative to MJO active envelope entrance to the MC.

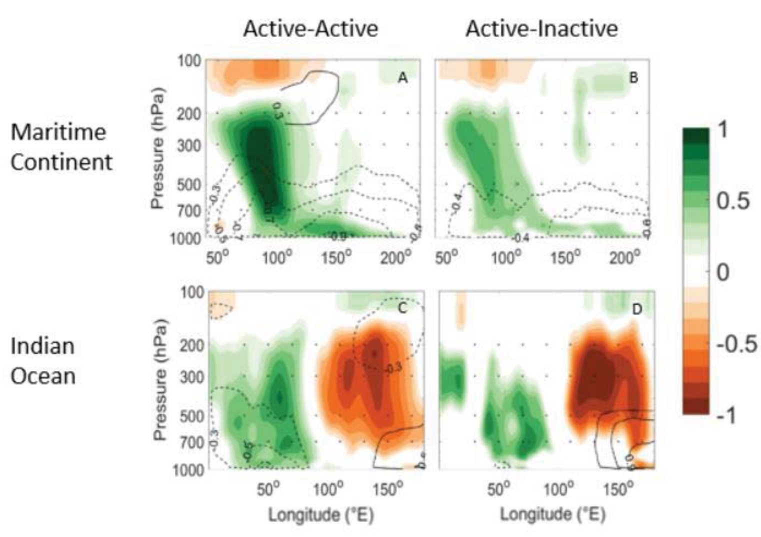

FIGURE 14: As in Fig. 13, but for background atmospheric anomalies during AA (panels a and c) and AI (panels b and d) MJO events over the MC (panels a and b) and Indian Ocean (panels c and d).

C. Comparing MJO amplitude changes to Quasi-Biennial Oscillation phase

The QBO-MJO interactions are analyzed in four main ways. First, relationships between QBO phase pair and atmospheric conditions such as zonal wind, vertical wind shear, and BV frequency are examined. Second, RMM amplitude differences by QBO phase pair are considered for the Indian Ocean, Maritime Continent, and western Pacific Ocean (MJO phases 2-7). Third, boreal winter RMM amplitude changes over the MC are investigated. Finally, seasonality of the QBO-MJO association is considered as the relationship between QBO and RMM amplitude change is contrasted by season. All results are presented first for the RMM index, then compared with results based on the OMI and BSISO indices.

Downward movement of the maximum zonal wind centers through the stratosphere is apparent in vertical profiles for each of the eight QBO phases (lettered A-H; Fig. 15). For example, during QBO phase A, there is an easterly wind maximum at 20 hPa (approximately 26 km in altitude above the Earth's surface) and a westerly wind maximum at 70 hPa (approximately 18 km). From QBO phases B to E, the lower-stratospheric westerly winds dissipate and the easterly winds propagate downward. By QBO phase E, these easterly winds are centered at 70 hPa, and upper-stratospheric westerly winds appear near 20 hPa and begin to propagate downward. From QBO phases F to H, the lower-stratospheric easterly winds dissipate and are replaced by the downward-propagating westerly winds, and upper-stratospheric easterly winds begin to develop, returning to QBO phase A conditions. This downward wind propagation is captured as counter-clockwise movement through the QBO phase space (downward movement in Fig. 15 corresponds to counterclockwise movement in Fig. 9).

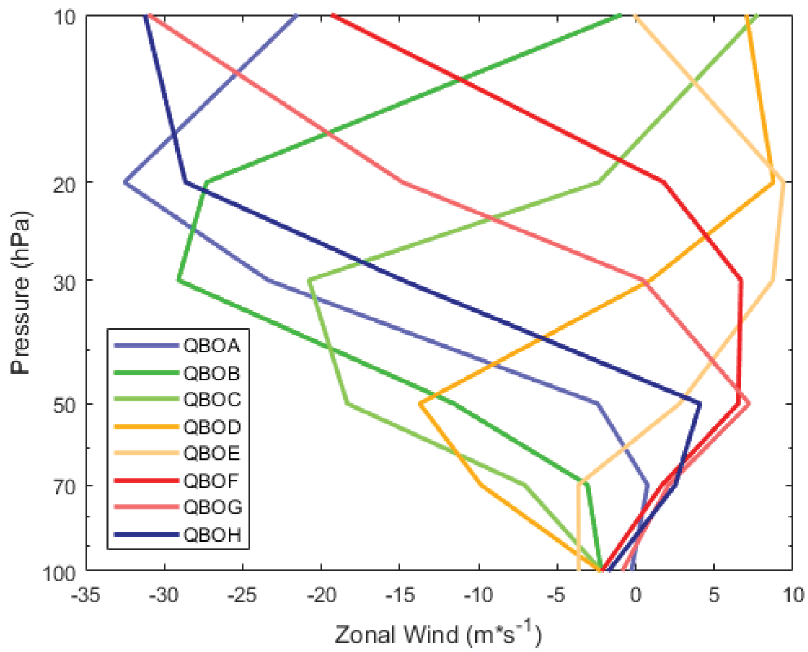

FIGURE 15: Mean (10°S-10°N, 0°E-360°E) zonal winds in all months from 1980-2017 for each of the eight QBO phases defined in Fig. 9.

Zonal wind speed at 70 hPa varies by up to 15 m s^{-1} (Fig. 15) across the eight QBO phases, but all eight QBO phases have similar zonal wind speeds at 100 hPa (near the tropopause). Therefore, zonal wind shear varies greatly among QBO phases. These significant differences persist when QBO phases are grouped into pairs (Section 2C). Zonal wind becomes more negative (positive) with height in the stratosphere, i.e. winds flow faster from the east (west) at the tropopause during QBOEM and QBOEL, (QBOWM and QBOWL), (Fig. 16a). The differences in zonal wind and zonal wind shear with QBO phase pair also extend to atmospheric stability (favorability for thunderstorm activity). Although stratospheric BV frequencies are positive (stable) for all phase pairs, their magnitudes vary by phase pair (Fig. 16b). Specifically, BV frequencies at 100 hPa (near the tropopause, the boundary between the troposphere and the stratosphere) are anomalously negative (indicating a less stable upper troposphere more conducive

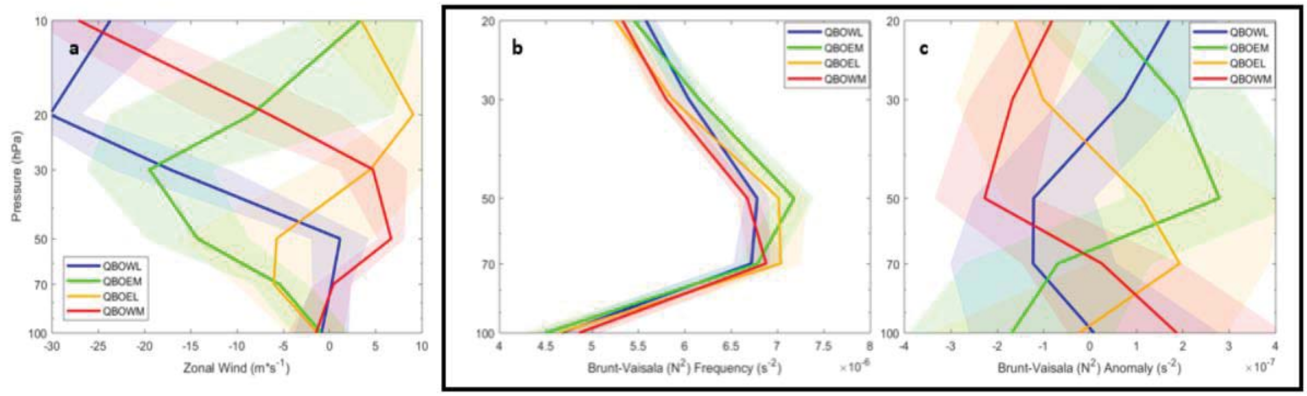

FIGURE 16: Boreal winter zonal wind speeds (a), mean Brunt-Vaisala (BV) frequency values (b) and BV anomalies (c) for each of the four QBO phase pairs from 1980-2017. Values within +/- 1 standard deviation are shaded, and BV anomalies were calculated relative to a 31-day sliding mean to minimize seasonal variability. Note the different y-axis scale between panel a and panels b and c, annotated with a black box surrounding panels b and c.

to thunderstorm activity) during QBOEM and anomalously positive (indicating a more stable upper troposphere less conducive to thunderstorm activity) during QBOWM (Fig. 16c). During QBOEL and QBOWL, BV frequency anomalies at 100 hPa are close to zero (indicating no noteworthy changes in upper-tropospheric stability).

Stratospheric temperature differences associated with each QBO phase are proportional to their respective zonal wind shear anomalies (Fig. 17). For example, during QBOEM, mid-stratospheric easterly winds correspond to negative zonal wind shear anomalies in the lower stratosphere. Conversely, during QBOWM, mid-stratospheric westerly winds are co-located with positive zonal wind shear values in the lower stratosphere. Baldwin et al. (2001) explained that QBO-linked temperature anomalies are in thermal wind balance with QBO-driven zonal wind shear. That is, those temperature anomalies can be related to zonal wind shear associated with the QBO via the thermal wind equation. At the equator, the thermal wind equation can be approximated as:

$$\frac{du}{dz} = -\frac{R}{H\beta}\,\frac{\delta^2 T}{\delta y^2} \tag{5}$$

where $\frac{du}{dz}$ is the zonal wind shear, R is the dry air gas constant, β is the change in Coriolis force with latitude, H is the scale height, T is the temperature in Kelvin, and y is the latitude (Holton and Hakim, 2013). Warmer equatorially-centered temperatures ($\frac{\delta^2 T}{\delta y^2} < 0$) are related to positive temperature anomalies ($T' > 0$), and colder equatorially-centered temperatures ($\frac{\delta^2 T}{\delta y^2} > 0$) are related to negative temperature anomalies ($T' < 0$). Because R, β, and H are always positive values, the thermal wind relationship (Equation 5) can be simplified to:

$$\frac{du}{dz} \propto T' \tag{6}$$

where *T'* is the air temperature anomaly associated with the zonal wind shear (Randel et al. 1999). Therefore, the negative lower-stratospheric zonal wind shear found during QBOEM corresponds to negative (colder) lower-stratospheric temperatures (which would decrease upper-tropospheric stability), and positive lower-stratospheric zonal wind shear during QBOWM corresponds to positive (warmer) temperatures (which would increase upper-tropospheric stability). This relationship does not extend down into the troposphere (Fig. 17), where winds are westerly from

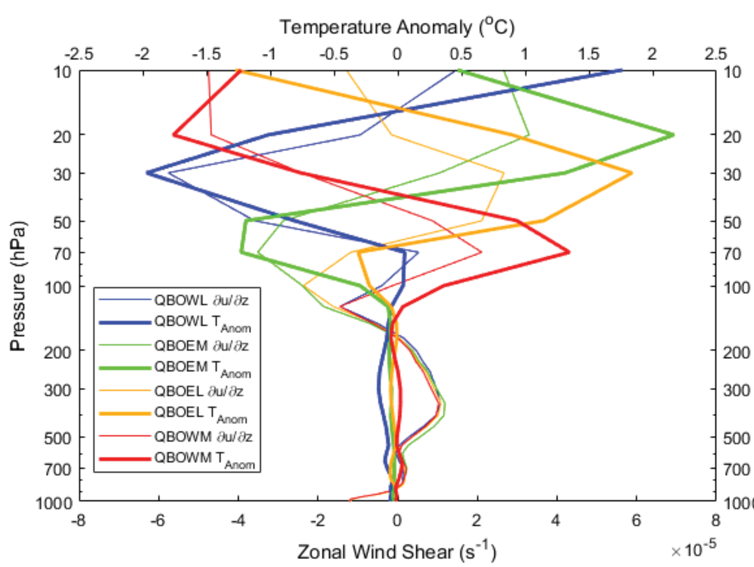

FIGURE 17: Mean (10°S-10°N, 0°E-360°E) zonal wind shear (s^{-1}; thin lines) and temperature anomalies (°C; thick lines) for the QBO phase pairs (QBOWL, QBOEM, QBOEL, and QBOWM), in all months from 1980-2017.

600 hPa to 200 hPa during all QBO phase pairs. Therefore, one important result from this analysis is that the physical mechanisms by which the QBO may affect MJO amplitude are concentrated primarily in the stratosphere.

During boreal winter, mean MJO RMM amplitude (mean of all MJO days) at the exit of MJO phase 5 is higher than mean RMM amplitude at the start of phase 4 during QBOEM (when mid-stratospheric winds are easterly). Conversely, mean RMM amplitude is lower at the exit of phase 5 than the start of phase 4 during QBOWM (when mid-stratospheric winds are westerly) (Figure 18a). That is, MJO events tend to strengthen (their RMM amplitudes increase) while moving across the MC during QBOEM, and MJO events tend to weaken (their RMM amplitudes decrease) while moving across the MC during QBOWM. This difference in final RMM amplitude occurs even though starting RMM amplitude was statistically identical for MJO days during both QBOEM and QBOWM (nearly 0.5, significant at the 95% confidence level). This difference indicates that during boreal winter, active MJO events strengthen while crossing the MC during QBOEM and weaken while crossing the MC during QBOWM. In contrast, MJO events during QBOEL and QBOWL do not develop significant RMM amplitude differences while moving over the MC. This is another important result of this work.

Because the MJO is both more active and slower moving during QBOEM than QBOWM (RMM amplitudes are greater than 1.0 on 75% of QBOEM days versus on 59% of QBOWM days), the above analysis was repeated for only MJO events for which the RMM amplitude remained greater than or equal to 1 (Fig. 18b). Additionally, RMM amplitudes for each MJO event were first binned and averaged by MJO phase before being averaged for all events in the same QBO phase pair in order to remove any effects of propagation speed (Section 2C). In these events, RMM MJO amplitudes are significantly larger during QBOEM than QBOWM in phase 5 (by 0.5 at the midpoint of phase 5), even though they are not statistically different from one another upon entrance to phase 4. This result is identical to the analysis that included all days of weaker propagating MJO events. Thus, RMM MJO amplitudes are significantly higher over the MC during QBOEM than QBOWM. The OMI MJO amplitudes exhibited similar changes over the western MC, but these differences did not reach a level of statistical significance until over the western Pacific Ocean. It is worth noting that these significant changes in RMM amplitude develop in RMM phases 4 and 5, but not 2 and 3 or 6 and 7. Therefore, the relationship between QBO and MJO amplitude changes for active events over the MC (and the seasonality of that relationship) is the focus of the remainder of this section.

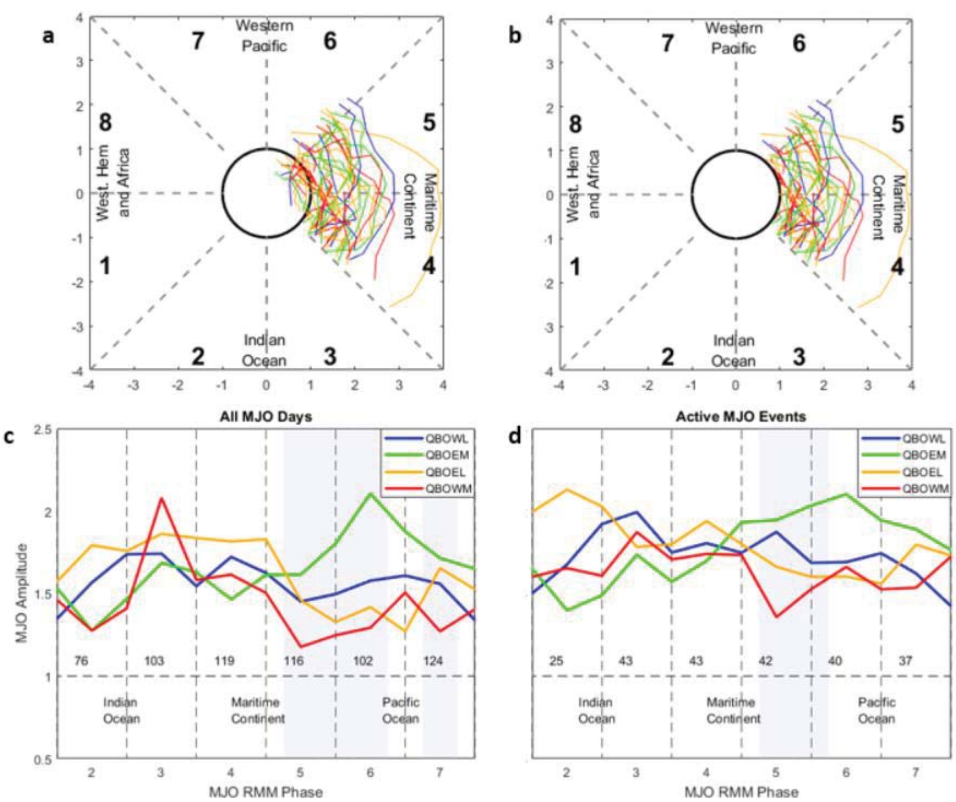

FIGURE 18: Mean RMM amplitudes of each QBO phase pair from MJO phases 2-7 for all MJO days (c) and all active MJO events (d) which entered MJO phase 4 active during boreal winter (DJF) from 1980-2017. Numbers above the dashed line represent the sample size of MJO event datapoints at the center of each phase. Shading denotes MJO phases where RMM amplitudes for QBOEM and QBOWM are statistically significant from one another, as indicated with a Welch's *t*-test. Phase space diagrams show all MJO event data over the MC included in each analysis (panels a and b, corresponding to panels b and d, respectively).

To better understand differences in MJO amplitude presented in the previous section, the RMM amplitude change of MJ O events was explored next (Table 3). The 42 initially active MJO events that moved through RMM phase 4 and 5 during boreal winter from 1980-2017 exhibited a mean amplitude change (ΔRMM) of -0.23. In other words, the RMM amplitude for each MJO event weakened on average by 0.23 while moving through the Maritime Continent. Ten of these events occurred during QBOEM, and those events strengthened by +0.14, or 0.37 above the long-term mean. The 11 events that occurred during QBOWM exhibited a mean RMM amplitude change of -0.49, or 0.26 below the long-term mean. This difference in amplitude change between QBOEM and QBOWM (MJO events in QBOEM strengthened over the MC +0.63 more than events during QBOWM, despite all events entering the MC active) is statistically significant at the 95% confidence level. Finally, during QBOWL and QBOEL (6 events and 15 events, respectively), MJO amplitudes weakened, but the weakening was small (within 0.09 of the climatological average).

Events identified with the OMI index showed a similar QBO relationship compared to the RMM index, except QBOEL events also weakened much more than the climatological average and QBOWL events also strengthened more than the climatological average. Specifically,

TABLE 3: Mean MJO RMM amplitude change over phases 4 and 5 for each QBO phase pair, for all MJO events which entered phase 4 active during boreal winter.

	ΔRMM	n	σ
ALL	-0.23	42	0.75
QBOWL	-0.14	6	0.67
QBOEM	+0.14	10	0.69
QBOEL	-0.32	15	0.81
QBOWM	-0.49	11	0.71

QBOEM events and QBOWL events strengthened by 0.25 and 0.20 more than the climatological average (weakening by 0.14), respectively. However, QBOWM and QBOEL events weakened by 0.31 and 0.15 more than the climatological average, respectively.

The thermal structure of the stratosphere was examined to better understand the differences in both amplitude and amplitude changes by QBO phase. During QBOEM, zonal wind shear was negative in the lower stratosphere, mean RMM amplitude of MJO days was greater (Figure 18; and consistent with Son et al. 2017), and active MJO events strengthened while moving over the MC (Table 3). This strengthening is consistent with colder lower-stratospheric temperatures (in thermal wind balance with the negative zonal wind shear). The resulting decreases in stability (and lower BV frequency) in the upper troposphere and lower stratosphere (UTLS) strengthen the intensity of deep convection associated with the MJO active envelope increase the zonal circulations in the equatorial troposphere associated with the MJO, and thus increase RMM amplitudes. Conversely, during QBOWM, zonal wind shear is positive in the lower stratosphere, MJO amplitude is decreased, and active MJO events weaken over the MC. This weakening is consistent with warmer lower-stratospheric temperatures (in thermal wind balance with the positive zonal wind shear). The resulting increases in UTLS stability (and higher BV frequency) weaken the intensity of deep convection associated with the MJO active envelope, decrease the zonal circulations in the equatorial troposphere associated with the MJO, and thus decrease RMM amplitude.

The relationship between RMM amplitude changes and QBO phase is found to reverse during boreal spring and summer (Figure 19). As discussed previously, during boreal winter, MJO events that cross the MC tend to strengthen during QBOEM and weaken during QBOWM (Figure 8; difference of +0.63 between QBOEM and QBOWM). However, during boreal spring, MJO events that cross the MC tend to weaken during QBOEM (Figure 19; by -0.36 more than climatology). During boreal summer, no QBO phase exhibits statistically significant changes in RMM amplitude (Figure 19). That seasonal shift from winter to summer is affected by one of the weaknesses of the RMM index, that it does not effectively capture intraseasonal variability of convection in boreal summer (Lee et al. 2013). To explore QBO influences on convection in boreal summer, the analysis was extended to a BSISO index (Kikuchi et al. 2012). During boreal summer, BSISO events that move northeastward across the MC and southeastern Asia tend to weaken during QBOEM (Figure 19; by -0.2 more than the climatology). This BSISO-based result is different from the change in RMM amplitude. Also, during boreal summer, OMI MJO events weaken while crossing the MC during QBOEM (but not to a degree of statistical significance), and strengthen while crossing the MC during QBOWM.

To explore potential physical mechanisms supporting those observed seasonal differences in RMM, OMI, and BSISO amplitude changes, zonal winds and BV frequencies were compared

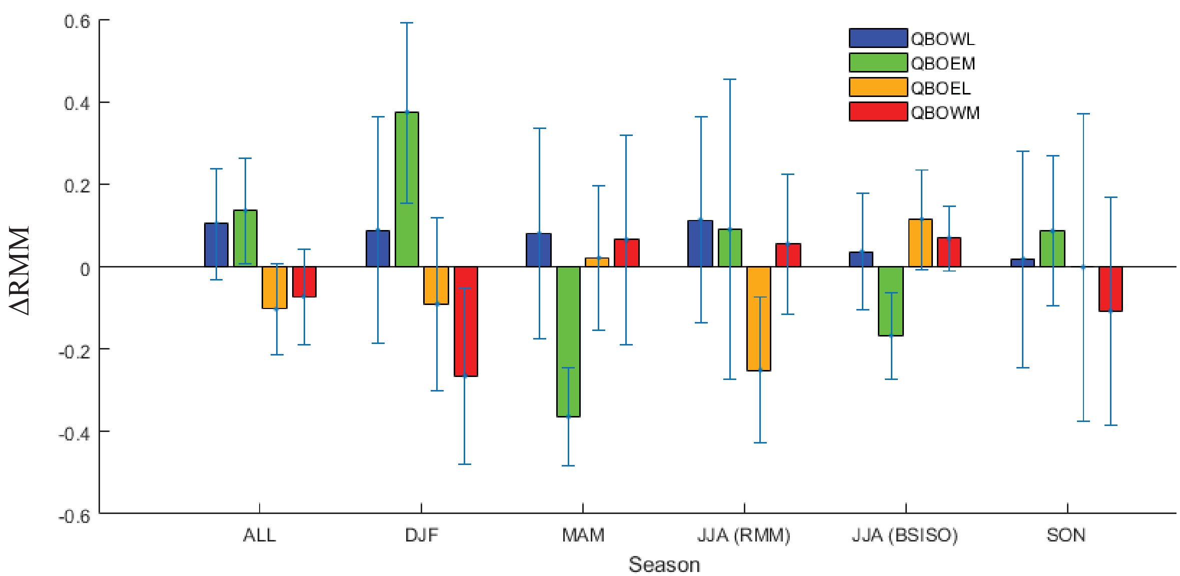

FIGURE 19: Mean amplitude change difference from climatological (1980-2017) average for initially active MJO events, binned by QBO phase pair and seasonal subset. Amplitude changes are presented for the full year (ALL), December-February (DJF), March-May (MAM), June-August (JJA), and September-November (SON). Boreal summer (JJA) analysis is repeated using MJO RMM amplitudes and BSISO amplitudes.

for boreal winter (DJF) and boreal spring and summer (MAMJJA). Spring and summer months were grouped together because of the similar QBO-MJO and QBO-BSISO relationships apparent in the RMM and BSISO indices for boreal spring and summer, respectively. Zonal winds and BV frequencies vary seasonally (Figure 20). Lower-stratospheric zonal wind (100 hPa to 70 hPa; Figures 20 a,b) under QBOEM conditions becomes more easterly with height during boreal winter (from -0.9 ms^{-1} at 100 hPa to -5.4 ms^{-1} at 70 hPa) than it does during boreal spring and summer (from -2.9 ms^{-1} at 100 hPa to -4.3 ms^{-1} at 70 hPa). These differences in zonal wind shear are associated with a more stable UTLS with smaller changes in stability by QBO phase. To date, no mechanisms have been proposed to account for this boreal summer relationship, and although lower-stratospheric stability exhibits some seasonal variability, other factors such as MJO seasonality may play a role in the seasonal reversal of the MJO-QBO relationship.

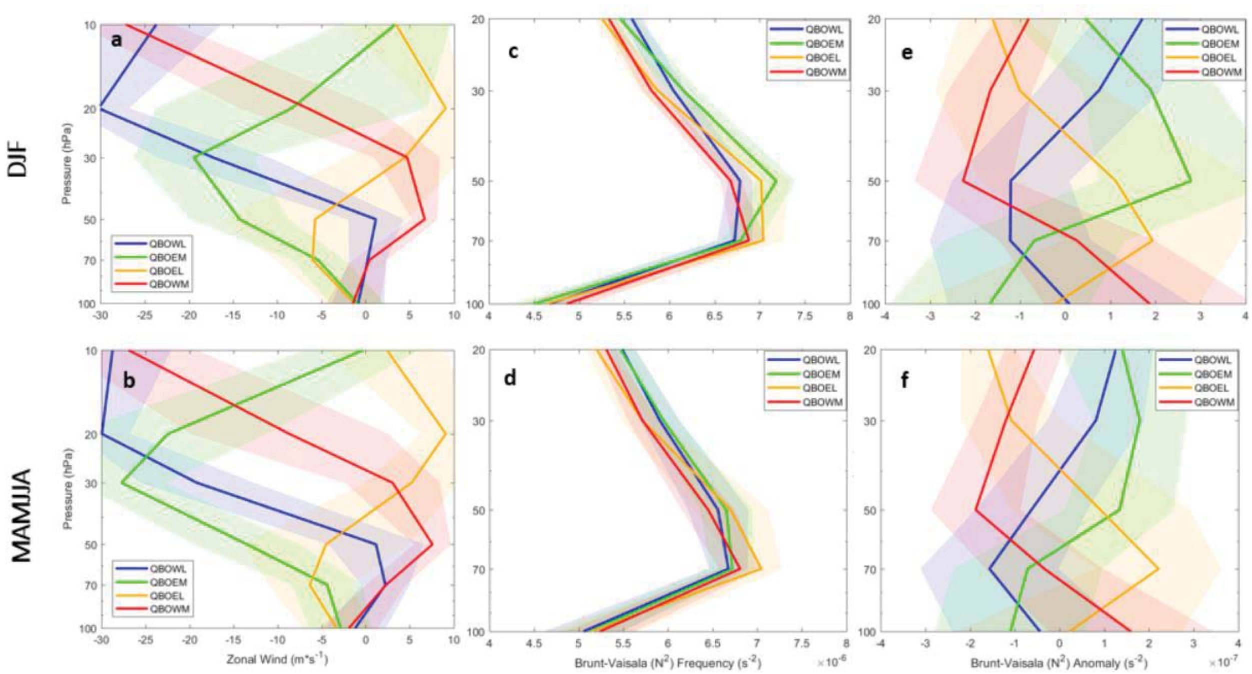

FIGURE 20: Zonal wind speeds (a,b), mean Brunt-Vaisala (BV) frequency values (c,d), and BV anomalies (e,f) for boreal winter (DJF; panels a,c,e) and boreal spring and summer (MAMJJA; panels b,d,f) based on a zonal mean (10°S – 10°N) from 1980-2017. Values within +/- 1 standard deviation are shaded, and BV anomalies were calculated relative to a 31-day sliding mean to minimize seasonal variability. Note the y-axis difference between panels a and b and panels c-f.

4. Conclusions

Relationships between the MJO and the large-scale environment in both the troposphere and stratosphere were examined to better understand the physical mechanisms responsible for MJO intensity and propagation. In the troposphere, MJO events from 1980-2015, identified with the WH04 RMM index, were categorized as one of four cases based on activity at the entrance to and exit from three regions (the MC, IO, and WP). Seasonal and regional changes in frequency of these four cases was analyzed. Standard anomalies of specific humidity and geopotential height for each of the four cases over each of those three regions. The QBO was categorized as one of four phase pairs using an EOF analysis of stratospheric zonal winds from 1980-2017. Effects of the QBO on the upper troposphere and the lower stratosphere were considered, and the relationship between MJO events over the MC and QBO phase pair, as well as the seasonality of this relationship, were studied.

MJO eastward propagation is found to be influenced by a number of factors, to include the region over which the MJO is propagating, the seasonality of the MJO, the initial and subsequent strength of the MJO, and the background atmospheric specific humidity and geopotential height anomalies. AA and II MJO events are favored more over the IO and WP, compared to the MC. Over the MC, active MJO events have a higher likelihood of weakening and failing to successfully propagate than in the IO or WP (e.g., AI events are favored in the MC compared to the IO or WP). In addition, inactive MJO events have a higher likelihood of strengthening and propagating out of the MC than in the IO or WP (e.g., IA MJO events are favored more over II events over the MC). Finally, active MJO events are more likely to propagate (AA events) during boreal winter than boreal summer, but this seasonality is reduced over the MC compared to the IO and WP.

Noteworthy features of MJO propagation across the MC are apparent in differences in specific humidity between propagation and non-propagation among active events. The AA MJO events propagating over the MC have significantly stronger positive humidity anomalies within the active envelope before they cross into the MC. This difference is much greater for MJO events over the MC than for those over the IO. In addition, a low-level specific humidity "moisture foot" extends eastward ahead of the active envelope in active events propagating over the MC, but it is stronger by day 0 in AA events AI than in events. Because these differences in specific humidity occur at day 0 (before AI events are distinguishable from AA events in the RMM index), they represent a potential method to aid in operationally distinguishing between MJO events that may or may not propagate at a later time. Moreover, these moisture foot signatures do not appear in any composites of initially active events over the IO or WP, and are therefore unique to the MC. Geopotential height anomalies also exhibit significant differences among MJO cases before shifts in activity are detected by the RMM index. Propagating events (regardless of initial activity) are characterized by more negative lower-level and more positive upper-level height anomalies. These height anomalies may indicate that MJO circulation within the active envelope is stronger for the propagating events, but that this difference in strength is not immediately detected by the RMM index.

Finally, an empirical orthogonal function analysis was developed and then employed to categorize QBO conditions into one of four phase pairs (QBOWL, QBOEM, QBOEL, and QBOWM) based on the vertical structure of zonal wind. The QBO phase pairs were then used to analyze MJO amplitude and changes in amplitudes, based on the WH04 RMM Index. Amplitude changes for MJO events in phases 4 and 5 were analyzed for boreal winter, and then again for boreal spring, summer, and autumn using the RMM, OMI, and BSISO indices. Vertical profiles of zonal wind speed and wind shear, temperature, and BV frequency were compared for the four

QBO phase pairs, and seasonality of zonal wind profiles and BV frequencies was analyzed by comparing DJF and MAMJJA composites.

During boreal winter, MJO amplitudes exhibit a relationship with QBO phase pair over the Maritime Continent (MC). During QBOEM (easterly mid-stratospheric zonal winds), active MJO events increase in RMM amplitude while moving through phases 4 and 5. During QBOWM (westerly mid-stratospheric zonal winds), MJO events decrease in RMM amplitude over the same phases. This difference occurs despite both sets of events having statistically indistinguishable RMM amplitudes when entering phase 4. This result remains unchanged when inactive MJO days are excluded from the analysis, thus contributing to the complex QBO-MJO relationship presented in Zhang and Zhang (2018). Thus, boreal winter MJO events are not only stronger in RMM phase 5 during QBOEM than during QBOWM, they also strengthen while moving through RMM phase 4 and 5 during QBOEM and weaken during QBOWM.

This boreal winter QBO-MJO amplitude and amplitude change relationship coincides with QBO-driven stability changes in the lower stratosphere (consistent with Yoo and Son 2016 and Son et al. 2017). That is, QBO-driven zonal wind shear drives temperature perturbations (in accordance with the thermal wind balance) and results in anomalously cold and warm mid-stratospheric conditions for QBOEM and QBOWM, respectively. Cold mid-stratospheric temperature anomalies and decreased near-tropopause stability during QBOEM likely enhance deep convection coupled with the MJO active envelope. Conversely, during QBOWM, warm mid-stratospheric temperature anomalies and increased near-tropopause stability likely weaken MJO active envelope-coupled deep convection. It is important to note that this process seems important only in boreal winter and only over the MC into the western Pacific Ocean (RMM phases 4-7), and not over the Indian Ocean (RMM phases 2 and 3) (in agreement with Zhang and Zhang 2018).

The QBO-MJO relationship is found to reverse with season. During boreal spring, MJO events moving across the MC during QBOEM conditions weaken more than the climatological average. However, MJO events amplitude changes over the MC during the other three QBO phase pairs (QBOEL, QBOWM, and QBOWL) are similar to the climatological average. During boreal summer, this relationship is not apparent in MJO amplitudes quantified with the WH04 RMM Index, potentially due to seasonally lower RMM amplitudes during boreal summer. Repeating the same analysis with a BSISO index yields results that mirror the boreal spring QBO-RMM relationship. That is, BSISO events weaken over the MC and southeastern Asia more than the climatological average during QBOEM, but not for the other three QBO phase pairs. Part of the seasonality of this QBO-MJO relationship may be explained by seasonality of near-tropopause stabilities. During boreal spring and summer, lower-stratospheric stabilities are not sharply reduced during QBOEM conditions. Other factors, such as seasonality of MJO strength and propagation, are likely factors in this seasonal reversal as well. Moreover, no mechanisms have been proposed to explain diminished boreal spring MJO and BSISO propagation during QBOEM. Further research is suggested to shed additional light on these mechanisms (e.g. QBO modulation of equatorial Kelvin and Rossby wave propagation and relationships with other atmospheric and oceanic variability that may affect MJO amplitude and propagation) and advance the meteorological community's understanding of the QBO-MJO relationship.

Works Cited:

Baldwin, M. P. and Coauthors, 2001: The quasi-biennial oscillation. *Rev. Geophys.*, **39**, 179-229, doi: 10.1029/1999RG000073.

Barrett, B. S., and C. R. Densmore 2016: More on the MJO relationship to US severe weather. *S2S Workshop*, Palisades, NY, Colombia University

Barrett, B. S., and L. M. Leslie, 2009: Links between tropical cyclone activity and Madden-Julian Oscillation phase in the North Atlantic and Northeast Pacific basins. *Mon. Wea. Rev.*, **137**, 727-744, doi:10.1175/2008MWR2602.1.

Barrett, B. S., and V. Gensini 2013: Modulation of daily U.S. April-May tornado frequency by the Madden-Julian Oscillation. *Geophys. Res. Lett.*, **40**, 2790-2795, doi: 10.1002/grl.50522.

Barrett, B. S., C. R. Densmore, and P. Ray, 2018: Large-scale environmental differences in active and weakening MJO events. *Journal of Geophysical Research Atmospheres*, in review.

Birch, C. E., S. Webster, S. C. Peatman, D. J. Parker, A. J. Matthews, Y. Li, H. E. E. Hassim, 2016: Scale interactions between MJO and the western Maritime Continent. *J. Climate*, **29**. 2471-2492, doi: 10.1175/JCLI-D-15-0557.1.

Dee, D.P. and Coauthors, 2011: The ERA-Interim reanalysis: configuration and

Feng, J., T. Li, and W. Zhu, 2015: Propagating and nonpropagating MJO events over Maritime Continent, *J. Climate*, **28**, 8430–8449. doi: 10.1175/JCLI-D-15-0085.1.

Hall, J. D., A. J. Matthews, and D. J. Karoly, 2001: The modulation of tropical cyclone activity in the Australian region by the Madden-Julian Oscillation. *Mon. Wea. Rev.*, **129**, 2970-2982, doi:10.1002/joc.4012.

Henderson, G. R., B. S. Barrett, and D. M. LaFleur, 2014: Arctic sea ice and the Madden-Julian Oscillation (MJO). *Climate Dynamics*, **43**, 2185-2196, doi: 10.1007/s00382-013-2043-y.

Holton, J. R., and G. J. Hakim, 2013: *An Introduction to Dynamic Meteorology, 5th Edition*, Academic Press, 532 pp.

Inness, P. M., and J. M. Slingo, 2006: Simulation of the Madden-Julian Oscillation in a coupled general circulation model. *J. Climate*, **132**, 1645-1667, doi: 10.1256/qj.05.102.

Kikuchi, K., B. Wang, and Y. Kajikawa, 2012: Bimodal representation of the tropical intraseasonal oscillation. *Climate Dyn.*, **38**, 1989-2000, doi: 10.1007/s00382-011-1159-1.

Kiladis, G. N., J. Dias, K. Straub, M. Wheeler, S. Tulich, K. Kikuchi, K. Weickmann, and M. Ventrice, 2014: A comparison of OLR and circulation-based indices for tracking the MJO. *Mon. Wea. Rev.*, **142**, 1697-1715

Kim, D., J. S. Kug, and A. H. Sobel, 2014: Propagating versus nonpropagating Madden-Julian Oscillation events. *J. Climate*, **27**, 111-125, doi: 10.1175/JCLI-D-13-00084.1.

Lawrence, D. M., and P. J. Webster, 2002: The boreal summer intraseasonal oscillation: Relationship between northward and eastward movement of convection. *J. Atmos. Sci.,* **59**, 1593-1606, doi: 10.1175/1520-0469.

Lee J.Y., B. Wang, M. C. Wheeler, X. Fu, D. E. Waliser, and I.S. Kang, 2013: Real-time multivariate indices for the boreal summer intraseasonal oscillation over the Asian summer monsoon region. *Climate Dyn.*, **40**, 493-509, doi: 10.1007/s00382-012-1544-4.

Lindzen, R. S., and A. R. Holton, 1968: A theory of the Quasi-Biennial Oscillation. *J. Atmos. Sci.,* **25**, 1095-1107.

Liu, C. B. Tian, K.-F. Li, G. L. Manney, N. J. Livesey, Y.L. Yung, and D. E. Waliser, 2014: Northern Hemisphere mid-winter vortex-displacement and vortex-split stratospheric sudden warmings: Influence of the Madden-Julian Oscillation and Quasi-Biennial Oscillation. *J. Geophys. Res.*, **119**, 12599-12620, doi: 10.1002/2014JD021876.

Liu, P., Q. Zhang, Y. Zhu, M. Khairoutdinov, H. Kim, C. Schumacher, and M. Zhang, 2016: A revised real-time multivariate MJO index, *Mon. Wea. Rev.,* **144**, 627-642, doi: 10.1175/mwr-d-15-0237.1.

Madden, R. A., 1979: Observations of large-scale travelling Rossby waves. *Rev. of Geophys*., **17**, 1935-1949, doi: 10.1029/RG017i008p01935.

Madden, R. A., and P.R. Julian, 1971: Detection of a 40-50 day oscillation in the zonal wind in the tropical Pacific. *J. Atmos. Sci.*, **28**, 702-708, doi: 10.1175/1520-0469(1971)028.

Madden, R. A., and P.R. Julian, 1972: Description of global-scale circulation cells in the tropics with a 40-50 day period. *J. Atmos. Sci.*, **29**, 1109-1123, doi: 10.1175/1520-0469(1972)029.

Madden, R. A., and P.R. Julian, 1994: Observations of the 40-50 day tropical oscillation: a

Marshall, A. G., H. H. Hendon, S. W. Son, and Y. Lim, 2017: Impact of the quasi-biennial oscillation on predictability of the Madden-Julian oscillation. *Climate Dyn.*, **49** 1365-1377, doi: 10.1007/s00382-016-3392-0.

Matsuno, T., 1966: Quasi-geostrophic motions in the equatorial area. *J. Meteor. Soc. of Japan*., **44**, 25-43.

Moncrieff, M. W., M. A. Shapiro, J. M. Slingo, and F. Moltini, 2007: Collaborative research at the intersection of weather and climate. *Bull. World. Meteor. Org.*, **56**(3).

Neale, R., and J. Slingo, 2003: The Maritime Continent and its role in the global climate: A GCM Study, *J. Climate*, **16**, 834-848, doi: 10.1175/1520-0442(2003)016.

Neena, J. M., J. Y. Lee, D. Waliser, B. Wang, and X. Jiang, 2014: Predicability of the Madden-Julian Oscillation in the Intraseasonal Variability Hindcast Experiment (ISVHE). *J. Climate*., **27**., 4531-4543, doi: 10.1175/JCLI-D-13-00624.1.

Nishimoto, E. and S. Yoden, 2017: Influence of the stratospheric Quasi-Biennial Oscilation on the Madden-Julian Oscillation during austral summer. *J. Atmos. Sci.*, **74**, 1105-1125, doi: 10.1175/JAS-D-16-0205.1.

Office of Naval Research (ONR), 2015: Propagation of Intra-Seasonal Tropical Oscillations (PISTON). Department of the Navy.

Pacific. *Mon. Wea. Rev.*, **120**, 407-429, doi: 10.1175/1520-0493(1992)120.

performance of the data assimilation system. *Quart. J. Roy. Meteor. Soc.*, **137**. 553-597, doi:10.1002/qj.828.

Ramage, C. S., 1968: Role of a tropical “Maritime Continent” in the atmospheric circulation, *Mon. Wea. Rev.,* **96**, 365-370, doi: 10.1175/1520-0493(1968)096.

Randel, W. J., F. Wu, R. Swinbank, J. Nash, and A. O’Neil, 1999: Global QBO circulation derived from UKMO stratospheric analyses. *J. Atmos. Sci.*, **56**, 457-474, doi: 10.1175/1520-0469(1999)056<0457:GQCDFU>2.0.CO;2.

Ray, P., and C. Zhang, 2010: A case study of the mechanics of extratropical influence on the initiation of the Madden-Julian Oscillation, *J. Atmos. Sci.*, **67**, 515-528, doi/10.1002/qj.765.

review, *Mon. Wea. Rev.*, **122**, 814-836, doi: 10.1175/1520-0493(1994)122.

Son, S. W., Y. Lim, C. Yoo, H. Hendon, and J. Kim, 2017: Stratospheric control of the Madden-Julian Oscillation, *J. Cli.*, **30**, 1909-1922, doi: 10.1175/JCLI-D-16-0620.1.

Sperber, K., 2003: Propagation and the vertical structure of the Madden-Julian Oscillation. *Mon. Wea. Rev.*, **131**, 3018-3037, doi: 10.1175/1520-0493(2003)131.

Stull, R. B. 1995. Meteorology Today for Scientists and Engineers. 385 pp.

Sui, C. and K. Lau, 1992: Multiscale phenomena in the tropical atmosphere over the western

Wallace, J. M., R. L. Panetta, and J. Estberg, 1993: Representation of the Equatorial Stratospheric Quasi-Biennial Oscillation in EOF Phase Space. *J. Atmos. Sci.*, **50**, 1751-1762, doi: 10.1175/1520-0469.

Wheeler, M., and H. Hendon, 2004: An all-season real-time multivariate MJO index: Development of an index for monitoring and prediction. *Mon. Wea. Rev.*, **132**, 1917-1932, doi: 10.1175/1520-0493(2004)132.

Yoo, C. and S. W. Son, 2016: Modulation of the boreal wintertime Madden-Julian Oscillation by the stratospheric quasi-biennial oscillation. *Geophys. Res. Lett.,* **43**, 1392-1398, doi: 10.1002/grl.v43.3.

Zhang, C. and B. Zhang, 2018: QBO-MJO Connection, *J. Geophys. Res.*, doi: 10.1002/2017JD028171.

Zhang, C., 2005: Madden-Julian Oscillation, *Rev. Geophys.,* **43**, doi: 10.1029/2004RG000158

Zhang, C., 2013: Madden-Julian Oscillation: Bridging Weather and Climate, *Bull. Amer. Meteor. Soc.,* **94**, 1849-187, doi: 10.1175/BAMS-D-12-00026.1.

Appendix: Glossary of Meteorological Terms

Boreal- pertaining to the Northern Hemisophere

Boreal Summer Intraseasonal Oscillation (BSISO)- a boreal summer version of the MJO, in which a nortwestward-tilted band of thunderstorm activity moves northeast over the Maritime Continent and southeastern Asia

Brunt Väisälä (BV) Frequency- the frequency at which a parcel of stable air will oscillate if moved from its initial position. BV frequency is a commen metric used to describe an air parcel's stability

Convection- thunderstorm and precipitation due to upward vertical atmospheric motion

Divergence- air flow away from a point

Geopotential Height- approximation of altitude of air at a given pressure

Kelvin Waves- zonally or poleward-propagating variations in upper-level winds which travel along a boundary (topographical or the equator) with wavelengths on the order of 1,000 km

Latent Heat- heat energy released or absorbed by water when undergoing a phase change

Meridional- in the North-South direction

Madden Julian Oscillation (MJO)- Shift in thunderstorm and zonal wind activity which moves eastward around the equator every 30-60 days

Maritime Continent- Region of island nations in southeastern Asia, including Indonesia, Papua New-Guinea, and the Philippines, characterized by unique topography and thunderstorm activity

Outgoing Longwave Radiation (OLR)- function of a cloud top's temperature. Indicates approximate cloud height and is a common measure of convective activity

Potential temperature- the temperature which an air parcel would reach if brought from its current altitude to sea level, due to pressure-driven (adiabatic) temperature changes

Quasi-Biennial Oscillation (QBO)- Reversal of zonal winds in the stratosphere above the equator every 2.5 years. Winds driven by the QBO are categorized in this study as QBOEM, QBOEL, QBOWM, and QBOWL, based on wind conditions defined in section 2C.

Radiosonde- Instrument which measures vertical profiles of the atmosphere, at a minimum generally including data on temperature, humidity, pressure, and wind speeds

Rossby Waves- zonally propagating meanderings in upper-level winds with wavelengths on the order of 10,000 km

Specific Humidity- humidity calculated as mass of water vapor per mass air ($kg*kg^{-1}$)

Stability- A description of how prone an air parcel is to convection, where more stable air parcels are less prone to convection

Subsidence- net vertical downward motion

Synoptic Scale- Occurring geospatially over 100-1000 km and temporally over days to weeks

Teleconnection- link between meteorological patterns separated by a long distance (~1,000 km)

Tropopause- Altitude at which the troposphere and stratosphere meet, approximately 16 km at the equator

UTC- Coordinated Universal Time, time zone synonymous with Greenwich Mean Time (GMT) and Zulu time (Z)

Wind shear- changes in wind speed and/or direction with height

Vorticity- quantification of flow rotating around a point

Zonal- in the East-West direction